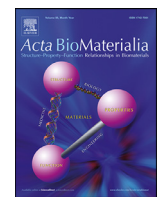




Contents lists available at ScienceDirect



Full length article

Microscale structural changes of individual fibrin fibers during fibrinolysis

Spencer R. Lynch^a, Sean M. Laverty^b, Brittany E. Bannish^b, Nathan E. Hudson^{a,*}^a Department of Physics, East Carolina University, 1000 E. 5th St., Howell-Sci-Physics-C209, Greenville, NC, USA^b Department of Mathematics and Statistics, University of Central Oklahoma, Edmond, OK, USA

ARTICLE INFO

Article history:

Received 22 September 2021

Revised 31 December 2021

Accepted 4 January 2022

Available online xxx

Keywords:

Fibrinogen

Hemostasis

Microscopy

Modeling

Plasmin

ABSTRACT

Fibrinolysis is the enzymatic digestion of fibrin, the primary structural component in blood clots. Mechanisms of fibrin fiber digestion during lysis have long been debated and obtaining detailed structural knowledge of these processes is important for developing effective clinical approaches to treat ischemic stroke and pulmonary embolism. Using dynamic fluorescence microscopy, we studied the time-resolved digestion of individual fibrin fibers by the fibrinolytic enzyme plasmin. We found that plasmin molecules digest fibers along their entire lengths, but that the rates of digestion are non-uniform, resulting in cleavage at a single location along the fiber. Using mathematical modeling we estimated the rate of plasmin arrival at the fiber surface and the number of digestion sites on a fiber. We also investigated correlations between local fiber digestion rates, cleavage sites, and fiber properties such as initial thickness. Finally, we uncovered a previously unknown tension-dependent mechanism that pulls fibers apart during digestion. Taken together these results promote a paradigm shift in understanding mechanisms of fibrinolysis and underscore the need to consider fibrin tension when assessing fibrinolytic approaches.

Statement of significance

We developed a method for interrogating lysis of individual fibrin fibers, enabling the time-resolved observation of individual fiber digestion for the first time. Our results resolve longstanding disagreements about fibrinolytic processes and reveal previously unknown mechanisms that also play a role. Also, we developed the first microscale mathematical model of plasmin-fibrin interaction, which predicts the number of plasmin molecules on each fiber and can serve as a framework for investigating novel therapeutics.

© 2022 The Authors. Published by Elsevier Ltd on behalf of Acta Materialia Inc.

This is an open access article under the CC BY-NC-ND license
(<http://creativecommons.org/licenses/by-nc-nd/4.0/>)

1. Introduction

Wound healing requires a proper balance of hemostasis and fibrinolysis. Coagulation, the final step of the hemostatic process, results in the creation of a blood clot containing a fibrin mesh network that stems the flow of blood, while the fibrinolytic process digests the fibrin fibers composing the network, restoring vascular flow. Imbalance in either of these processes can lead to occluded blood vessels resulting in pathological conditions including my-

ocardial infarction and ischemic stroke, which are leading causes of death and disability [1].

Fibrinolysis is a natural process involving a complicated system of promoters and inhibitors [2]. Plasmin, the primary enzyme responsible for the digestion of fibrin fibers, is activated from its inactive precursor plasminogen by either urokinase plasminogen activator (uPA) or tissue plasminogen activator (tPA).

One clinical approach to resolving an occluded blood vessel is to administer enzymes from outside the thrombus in a process called thrombolysis. While recombinant tPA is the standard thrombolytic agent used to treat strokes [3], a phase 1/2a safety study has shown potential for using plasmin as a thrombolytic [4]. Clinical studies have shown a limited time window for the safe ad-

* Corresponding author.

E-mail addresses: lynchsp18@students.ecu.edu (S.R. Lynch), slaverty@uco.edu (S.M. Laverty), bbannish@uco.edu (B.E. Bannish), hudsonn16@ecu.edu (N.E. Hudson).

ministration of tPA treatments for stroke (within 4.5 h after symptom onset) [5], and recanalization of the occluded blood vessel is often not achieved in thrombolytic treatments [6,7]. Thus, there is an important need for continued clinical assessments of safe thrombolytic approaches as well as basic biology studies to understand the mechanisms regulating fibrinolysis/thrombolysis.

In particular, there has been a dearth of studies aimed at elucidating the mechanisms by which fibrin fibers are digested. Fibrin fiber polymerization begins when thrombin cleaves specific residues in fibrinogen molecules, converting them to fibrin. Fibrin molecules then polymerize into half-staggered, double-stranded protofibrils, which laterally aggregate to form thicker fibers and a branched fibrin mesh. The conversion from fibrinogen to fibrin also exposes cryptic plasminogen, plasmin, and tPA binding sites [8,9]. However, once the binding sites emerge, the routes plasmin takes to digest the fibers and the structural and biophysical properties regulating fiber digestion are unresolved.

This knowledge gap remains, in part, because most fibrinolysis studies focus on the digestion of fibrin networks/clots and lack the spatial or temporal resolution to investigate fiber digestion. Previous studies have debated whether plasmin digests fibers along their entire length, leading to a uniform decrease in fiber diameter [10–12], or whether once the first plasmin molecule begins digesting at one site, feedback mechanisms promote direct digestion across the fiber leading to transverse cleavage [13–17]. A recent study suggested that fibers may swell during an initial phase of lysis as internal fiber associations are cut, after which the fiber fragments and is eventually cleaved through [18].

Formerly, we introduced the first assay to study the cleavage rates of individual fibers, but the assay lacked the spatial resolution to investigate mechanisms of fiber digestion [13,15]. In this study, we present an original approach to studying the mechanisms of individual fiber digestion using dynamic fluorescence microscopy. In our initial experiments we test whether fibers are uniformly digested or cleaved at one location and show that each fiber has multiple digestion sites. Next, we investigate the rate of digestion at each site and find that certain locations are digested faster than others, ultimately resulting in fiber cleavage at a single location. To understand whether our measured number of digestion sites is reasonable, we use mathematical models to estimate the number of plasmin molecules bound to the fiber at any time and find conditions that provide good agreement with experimental data. To determine the reason certain locations on the fiber are digested faster than others, we investigate correlations between local fiber digestion rates, cleavage sites, and fiber properties such as initial thickness. Importantly, we find that fibrin slides longitudinally along the fiber during digestion, suggesting that fibers are pulled apart. We show that inherent fiber tension [13,15,19,20] likely accounts for this observation and, therefore, plays an important role in regulating fibrinolysis. Taken together, these results resolve long-standing disagreements about fibrinolytic processes, reveal previously unknown mechanisms, and expose a need for a dramatic change in considering the role of fiber tension in regulating fibrinolytic outcomes.

2. Methods

2.1. Preparing and imaging samples

Fibrin fibers were polymerized between micropatterned ridges measuring 20 μm wide, 10 μm deep, and 20 μm apart as described previously [15]. Aliquots of unlabeled and ALEXA 488-labeled human fibrinogen were thawed from -80.0 °C and diluted to 2.0 mg/mL and 0.0308 mg/mL, respectively, using a HEPES Buffered Saline (HBS; 20mM HEPES, 150 mM NaCl, pH 7.4) and placed onto the ridged surface. Human alpha thrombin was added

to the fibrinogen solution with final concentrations of 0.1 U/mL and 1 mg/mL, respectively, in HBS with 5 mM Ca^{2+} , and the solution polymerized for an hour at 37 °C. Plasmin (final concentration 0.066 U/mL) was added to the samples right before imaging to initiate fibrinolysis.

2.2. Microscopy

Samples were placed face up on a Leica DMi8 epifluorescent microscope (Leica Microsystems Inc., Buffalo Grove, IL) and imaged with a 63x oil immersion objective. After the addition of plasmin, images were taken with a Leica DFC9000GT SCIMOS 4 Megapixel monochrome camera with each image measuring 2048 pixels. After the addition of plasmin, images of 211 μm^2 -sized areas were taken every 2.5 s for 10 min, after which all fibers were lysed, leading to a maximum time error of ± 1.25 s.

2.3. Image processing

Fibers were subject to strict exclusion/inclusion criteria for analysis (Supplement Sections A.1–A.5 and Supplemental Figs. 1–5). Images were manually segmented into separate time series, each containing a single fiber. Background noise was subtracted using FIJI/ImageJ's rolling ball method which was not found to significantly alter fiber intensity values [21]. Images were adjusted using FIJI/ImageJ's "rotate" and "crop" so that fibers were horizontal and included all fiber signal with an additional 5 pixels of either ridge [22]. Processed images were imported into MATLAB (The Mathworks Inc., Natick, MA) as 2D matrices containing fiber fluorescence intensity values horizontally and vertically discretized into one-pixel increments. Since fiber intensity correlates with fiber width, the average intensity value of a pixel column was treated as apparent fiber width [23]. The apparent width at each location along a fiber at one time point will be referred to as a cross-sectional intensity profile (Supplement Section A.3 and Supplemental Fig. 2). To look for correlations between fiber properties and for trends between fibers, we normalized each fiber's intensity and length values (Supplement Section A.6 and Supplemental Figs. 6&7).

2.4. Determining the rate of fiber digestion

Linear fits were applied to the cross-sectional intensity profile values over time at each location along the fiber using MATLAB's "polyfit" function and the resulting slope values correspond to the rate of change in cross-sectional intensity at that location. These digestion rates were plotted for each location on the fiber, representing the rate of change in the apparent fiber width over time versus location (Fig. 1). In MATLAB a spline was fit to digestion rates and prominent minima of the fit function, interpreted as digestion sites, were found using the MATLAB "islocalmin" function (Supplement Section A.7 and Supplemental Fig. 8A).

2.5. Mathematical model

We created a stochastic mathematical model, based on the experimental set-up described above, to estimate the time course of plasmin diffusion and binding (Supplement Section C). The model domain consisted of a fibrin free region through which plasmin could diffuse and four fibrin fibers to which plasmin could bind. At each time step, each plasmin molecule had a probability of diffusing, binding (if it was near a fiber), and unbinding (if it was bound). We recorded the location and bound/unbound status of each plasmin molecule at each time step, which allowed us to plot time courses of the number of bound plasmin molecules and to calculate the average time it took for plasmin to first bind to

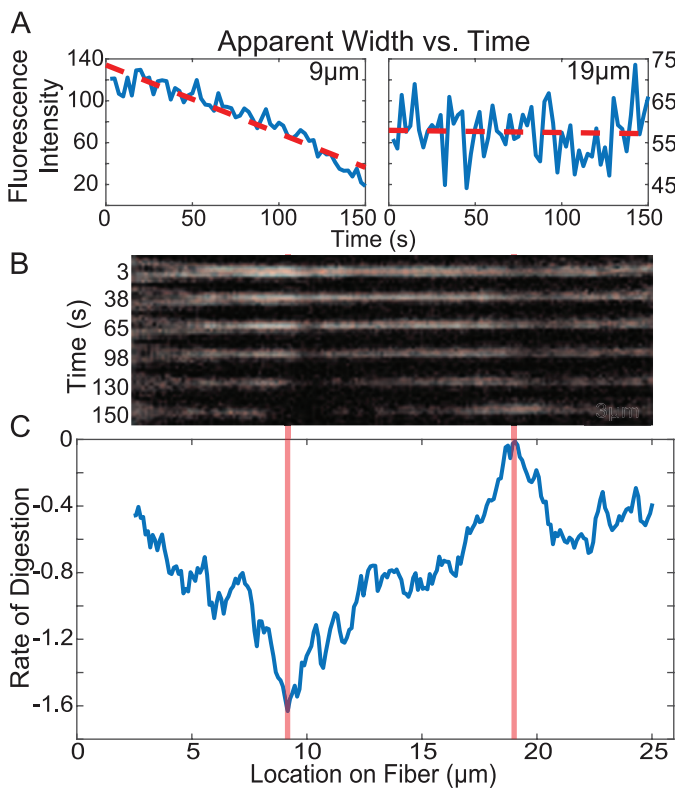


Fig. 1. Fiber Fluorescence Intensity and Digestion Rates. (A) Plots showing the average cross-sectional fluorescence intensity as a function of time for representative locations. Locations of 9 μm and 19 μm are shown, which correspond to the locations marked by the orange lines in panel B. Red lines show linear fits to the data which allow a quantification of the average rate of change of the fluorescence intensity, and hence the average rate of change of fiber diameter. (B) Snapshots of the fibrin fiber showing the fluorescence intensity along the fiber at different points in time. (C) The average rate of change of fluorescence intensity at every location along the fiber. Rate of digestion was calculated at each location as the slope of the fluorescence vs time plot at that location (red lines in panel A). (For interpretation of the references to colour in this figure legend, the reader is referred to the web version of this article.)

any fiber. We numerically solved a reaction diffusion master equation on a lattice using a kinetic Monte Carlo-like algorithm [24–26] with fixed time steps (Supplement Section C.5). The state of all plasmin molecules was updated at each fixed time step.

The model domain was a 3-dimensional square lattice (Supplemental Fig. 12A), 4 nodes wide and 60 nodes tall, with lattice edges connecting adjacent horizontal and vertical nodes, and with one lattice edge coming out of the plane of the page at each node. To best mimic the experimental conditions, the length of each edge was 20 μm (corresponding to the length of a fibrin fiber), and nodes were 0.0727 μm wide (corresponding to the diameter of a fibrin fiber). The bottom four 3-dimensional edges (highlighted in pink in Supplemental Fig. 12A), were assumed to be fibrin fibers, to which plasmin could bind. The remaining 652 edges, which we call "ghost edges", were simply used to demarcate space and were used for plasmin diffusion as described below. For simplicity, the model considered a small 3-D volume that was only 1 edge thick in the direction coming out of the page with imposed periodic boundary conditions in that dimension (no-flux boundary conditions were used in the horizontal and vertical dimensions). This periodic slab of clot was assumed to run between edge midpoints, so the 1-edge depth was actually composed of 2 halves of 2 separate edges.

A fixed number of plasmin molecules (Supplement Section C.4) were randomly uniformly distributed on the ghost edges. For simplicity, we assumed every plasmin molecule was at the midpoint

of the edge it occupied. At each time step, each plasmin molecule could diffuse to one of its 8 nearest neighbors (Supplemental Fig. 12B, fewer neighbors if plasmin was on the boundary) with equal probability or remain on the current edge, and if the plasmin molecule was on an edge containing fibrin, it could bind with some probability. Bound molecules had an unbinding probability at each time step, and unbound molecules on a fibrin fiber had a binding probability. The model algorithm is outlined in detail in Supplement Section C.5.

3. Results

3.1. Digestion rates

We interrogated the digestion rates at every location along the length of the fiber and refer to this as the change in apparent fiber width. Fig. 1A shows representative plots of the cross-sectional intensity vs time at two locations fit with the linear trend line whose slope is the digestion rate. Fig. 1C shows the rate of digestion at every location along the fiber. Digestion rates are not uniform along the fiber length, with some locations changing rapidly (more negative), while other locations have very little change in width (value closer to zero). This was true for all 60 fibers investigated with this approach.

3.2. Digestion and cleavage sites

To interrogate trends in fiber cleavage locations we generated a histogram of the normalized cleavage site locations (Fig. 2A) which shows that the cleavage site is not random, and that fibers were most likely to break 20–40% away from the fiber edges. We also investigated the number of digestion sites along the fiber (Fig. 2B and Supplemental Fig. 8) finding a mean number of 14 digestion sites with a range of 6–22 sites (Fig. 2B).

3.3. Cleavage times

Every included fiber was digested at multiple locations along its length before being transversely cleaved into two distinct parts. To quantify the time it took plasmin to cleave the fiber after arriving, we analyzed each frame for any movement in the fiber indicating that lysis had begun. Starting with the first frame where any movement/digestion was observed, we then measured the number of frames until the fiber was cleaved. Using a frame rate of 2.5 s/frame, we then converted this into the cleavage time for the fiber. Cleavage times (sample mean = 49.782 s, sample SD = 34.311, $n = 178$) are fitted by a gamma distribution with shape parameter $\alpha = 2.956$ and rate parameter $\beta = 0.059$, estimated simultaneously using the 'glm()' function in R [27]. The gamma distribution, a two-parameter distribution from the exponential family of distributions, has applications to event waiting times. The exponential distribution is a special case of the gamma distribution with a shape parameter $\alpha = 1$, corresponding to the waiting time until the first occurrence of an event at rate β . The gamma distribution gives the waiting time until the α th event, when each event occurs independently at an exponential rate β . A possible interpretation to this fit by the gamma distribution is that cleavage is the result of an underlying process, events of which take place independently at a rate of $\beta = 0.059$ per second, of which approximately three events ($\alpha = 2.95$) must occur before cleavage itself occurs. The fitted gamma distribution (blue) is superimposed on the raw empirical density (black) and histogram (gray) (Fig. 2C). To assess the fit visually, we show empirical density functions for each of twenty simulated datasets sampled from the fitted distribution (red curves) (Fig. 2C). Cleavage times were

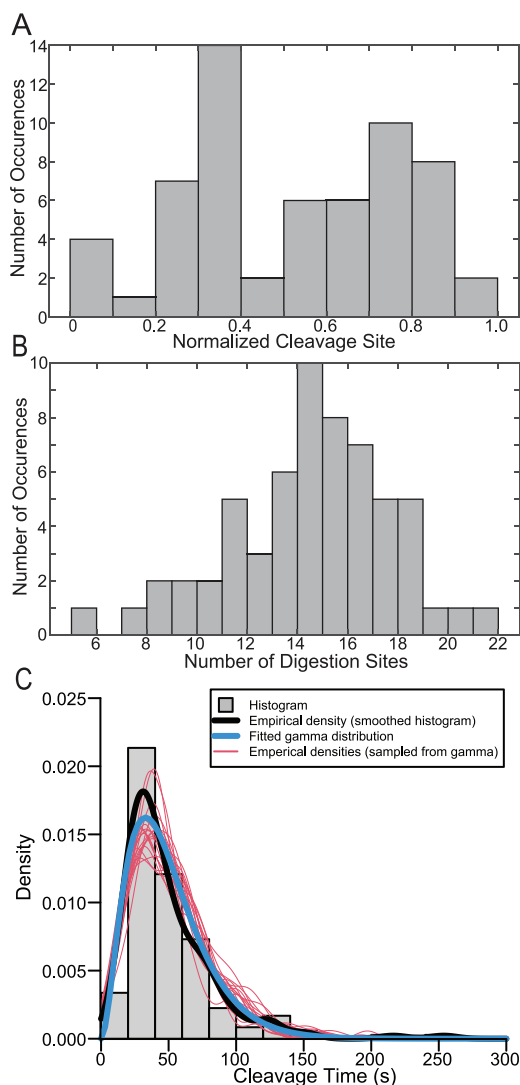


Fig. 2. Location of the Cleavage Site, Number of Distinct Digestion Sites and Cleavage Times. (A) Histogram showing the normalized location of cleavage sites of fibrin fibers. (B) Histogram showing the number of digestion sites on a single fibrin fiber. 60 fibers were used for these analyses. Locations were normalized as described in Supplemental Section A.6 and Supplemental Figs. 6&7. (C) Histogram showing the time taken for fibers to be cleaved (gray), as well as an empirical density function (black) corresponding to the continuously measured cleavage times, fitted gamma distribution (blue), and empirical density functions calculated for twenty independent samples (each of size $n = 178$) from the fitted gamma distribution (red). (For interpretation of the references to colour in this figure legend, the reader is referred to the web version of this article.)

used for all 178 fibers with the only selection criterion being transection of the fiber.

3.4. Mathematical model

To better understand the number of experimentally identified digestion sites, we used our mathematical model to plot the time course of the number of bound plasmin molecules on 40 distinct fibers (Fig. 3A). After 50 s (the experimental mean cleavage time), the model predicts between 5 and 27 bound plasmin molecules, with a mean of 14.25.

The model was also used to study the mean first passage time [28,29], or how long it takes plasmin to first bind to a fiber (Fig. 3B). We find that for model simulations initialized with 10^3 or more plasmin molecules uniformly distributed throughout the domain, the first plasmin binding always occurs within 1 sec-

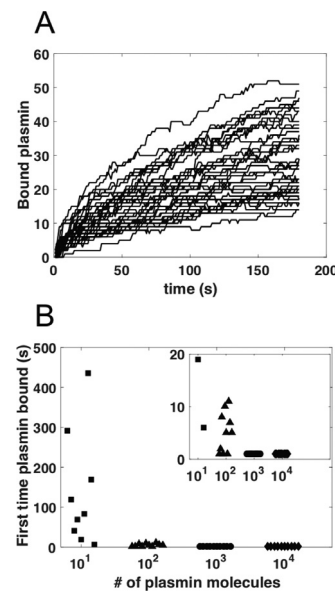


Fig. 3. Mathematical Model Results. (A) Time course of plasmin binding to fibrin fibers. Individual curves show the data for the number of plasmin molecules bound to a distinct fiber as a function of time. Simulations (which included 4 fibrin fibers) were initialized with 1426 plasmin molecules randomly distributed throughout the domain and were repeated 10 times. (B) The time at which plasmin first bound to any fiber, as a function of the order-of-magnitude number of plasmin molecules used in the simulation (details of plasmin number in Supplement Section C.4). 10 independent simulations were run for each plasmin amount. Inset is zoomed in version of larger figure. For both 10^3 and 10^4 plasmin molecules, plasmin first bound to a fiber within the first second in all 10 simulations.

ond (Supplemental Figs. 14&15). Reducing the number of plasmin molecules results in longer first binding times and more variability.

3.5. Correlations

We investigated correlations between fiber characteristics and digestion rates. First, we find no significant relationship between the location of the maximum rate of digestion and the location of the cleavage site (Fig. 4A). However, the site of the maximum rate of digestion and the location of the initially thickest part of the fiber (Fig. 4B) shows a stronger correlation. A weak negative correlation exists between the maximum digestion rate and the initially thinnest part of the fiber (Fig. 4C). Intriguingly, the initially thinnest part of the fiber never occurs in the middle, but rather in the 20% of the fiber closest to either end.

Additionally, we investigated correlations between fiber characteristics and the location of the cleavage site. We find very little correlation between the initially thickest and thinnest location of the fiber and the cleavage site (Fig. 5A&B). To investigate the importance of initial fiber width, we created a distribution of the normalized initial fluorescence intensity values at the cleavage site of every fiber (Fig. 5C). Cleavage sites most often correspond to thinner parts of the fiber, which have an initial relative width of roughly 20–40% of the maximum. Bins corresponding to the thickest ($> 70\%$) parts of the fiber are relatively unpopulated. We also investigated the distance between the cleavage site and the location of the maximum initial fiber width (Supplemental Fig. 10). While Fig. 5A confirms there is no correlation between cleavage site location and maximum initial intensity, Supplemental Fig. 10C additionally indicates that the relative distance between the cleavage site location and the location of maximum initial fiber width can be quite large. Thus, fibers are likely to be cleaved at thinner sites, but rarely the thinnest or thickest location on the fiber, and the cleavage sites can be close or far from the thickest part of the fiber.

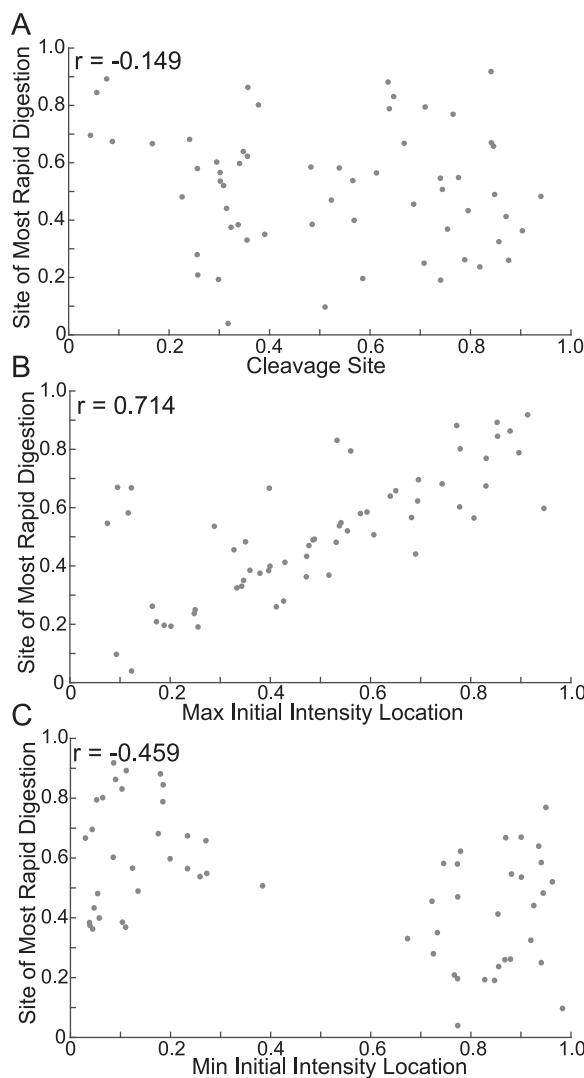


Fig. 4. Relationships Between Fiber Characteristics and Digestion Rates. (A) Scatter plot of the site of most rapid digestion vs cleavage site. (B) Scatter plot of the site of most rapid digestion vs the location of maximum initial intensity. (C) Scatter plot of the site of most rapid digestion vs the location of minimum initial intensity. 60 fibers were used for these analyses. All Pearson coefficients (r) were found with a 95% confidence interval. Locations were normalized as described in Supplemental Section A.6 and Supplemental Figs. 6&7.

3.6. Longitudinal fluorescence dynamics

Next, we analyzed trends in the cross-sectional fiber intensity at each location along the fiber during digestion. We observe that in the frame before digestion, the minimum in the intensity vs location plot corresponds with the observed cleavage site in the images (Fig. 6A&B, black curve). In the frame after the cleavage event, the ends of 52% of fibers appear to form a V-shaped, cone-like pattern (Fig. 6C). This cone-like structure persists for an average of 13.5 and maximum of 45 s after cleavage.

In analyzing time-series data (Fig. 1B and Supplemental movies) it appears that fluorescence intensity slides longitudinally along the fiber during digestion with a majority of the sliding occurring towards the end of digestion. We tracked the location of peaks in the cross-sectional fluorescence intensity profiles over time during digestion (representative intensity curves in Fig. 6A&B) and found that peaks shift over time, to the left and right. We tracked 95 peaks in 45 fibers over the last ~20 s of digestion and found that most peaks shifted 1.2 μm but shifts up to 6 μm were ob-

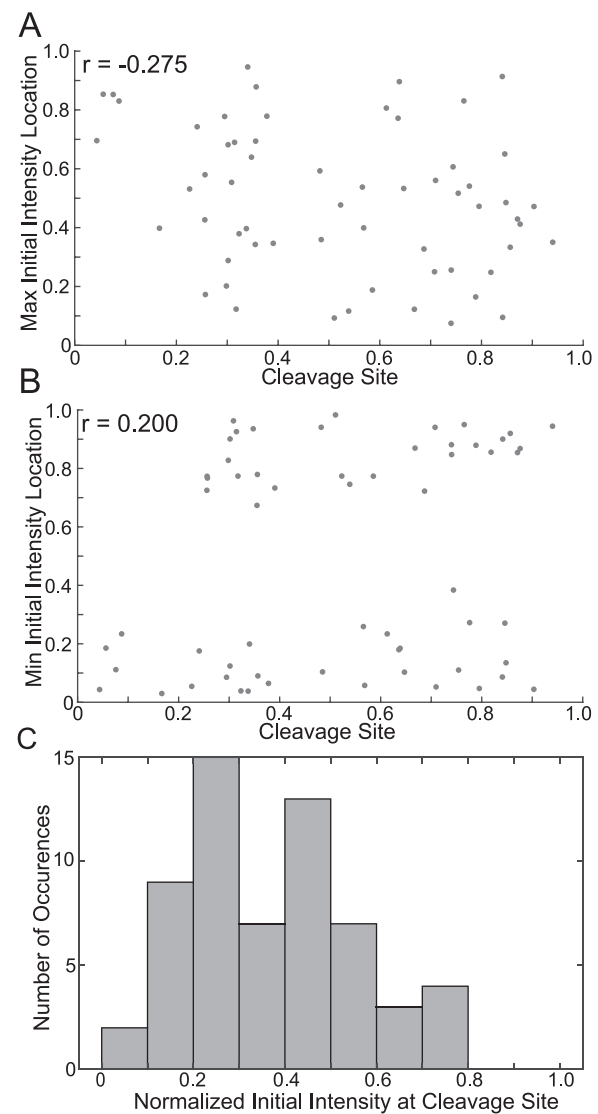


Fig. 5. Relationships Between Fiber Characteristics and Cleavage Sites. (A) Scatter plot of the site of initial maximum intensity vs cleavage site. (B) Scatter plot of the site of initial minimum intensity vs cleavage site. All Pearson coefficients (r) were found with a 95% confidence interval. (C) Histogram showing the normalized initial intensity at cleavage sites. 60 fibers were used for these analyses. Locations were normalized as described in Supplemental Section A.6 and Supplemental Figs. 6&7.

served (Fig. 6D). Peaks typically shift away from digestion sites (Fig. 6A&B). The initial direction of shifting does not determine the overall path of the intensity peak as shown by either green arrow in Fig. 6.

4. Discussion

The results from this study help to resolve longstanding disagreements on mechanisms of fiber digestion, while also revealing new mechanisms that may play dramatic roles in regulating fibrinolysis. Previous studies, primarily utilizing fluorescence and scanning electron microscopy (SEM), indicated that fibers were transversely cleaved at a single point [13–16,30]. Hence, it was suggested that the formation of free C-terminal lysines during plasmin digestion creates a feedback mechanism, recruiting additional plasmin molecules to digestion sites and causing transverse cleavage at those sites [17,31]. Additionally, geometrical considerations suggest that plasmin molecules can crawl between binding sites on protofibrils, which would also promote transverse cleav-

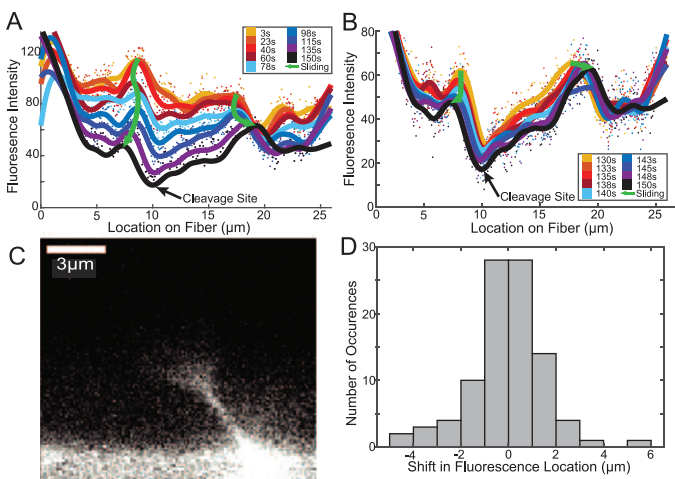


Fig. 6. Structural Evolution of a Representative Fiber. (A) Plot showing traces of the average cross-sectional fluorescence intensity for a representative fiber at multiple instances in time. Peaks in the traces change locations longitudinally along the fiber, termed fluorescence sliding. Two prominent peaks are marked with green arrows but are not the only fluorescence sliding occurring. (B) Plot showing a zoom-in of the data shown in panel A but looking at the average cross-sectional fluorescence intensity for the last 9 timepoints before cleavage. (C) The first frame after a fiber's cleavage shows a cone-like structure, such as the one seen in this representative image, in 52% of fibers. (D) Histogram showing the displacement of 95 peaks from 45 fibers in the last 20 s of their digestion. A negative shift represented a leftward movement, and a positive shift represented a rightward movement. (For interpretation of the references to colour in this figure legend, the reader is referred to the web version of this article.)

age [17,32,33]. On the other hand, studies primarily using turbidity and atomic force microscopy (AFM) have suggested that the diameter of fibrin fibers decreases uniformly during lysis due to plasmin molecules binding and digesting the fiber radially along its entire length [10–12].

Our results indicate that digestion does occur along the entirety of a fibrin fiber, but that digestion rates are nonuniform. The apparent digestion rates are actually a result of two phenomena: digestion by plasmin and fibrin longitudinal sliding. The loss of cross-sectional fluorescence intensity in our experiments (Figs. 1A & 6A&B) suggests that digestion by plasmin results in the loss of molecules or sections of protofibrils as plasmin severs their connections with the other parts of the fiber. The longitudinal shifting of the fluorescence intensity along the length of the fiber during digestion (Fig. 6A&B) indicates that fibrin molecules also slide along the fiber. Both processes result in local thinning of the fiber and contribute to its eventual cleavage. These results validate both transverse cleavage and radial digestion as mechanisms contributing to the lysis of fibrin fibers, but also expose their individual incompleteness as comprehensive descriptions of the process. A wholistic account of the mechanisms of fiber digestion must include non-uniform digestion along the length of the fiber by multiple molecules, digestion across the fiber by individual molecules, and the longitudinal sliding of fibrin.

Our experimental setup had two advantages over previous studies, which allowed these insights. First, with respect to previous fluorescence-based studies of lysis, our time resolution (2.5 s) was faster [30,32], allowing us to observe the digestion of single fibers. In addition, labeling our fibers with Alexa488 provided a more uniform fiber labeling than previous studies that used fluorescent microspheres [13,15,34], and likely resulted in less fiber elongation (data not shown). Second, unlike AFM-based experiments, where fibers are adsorbed to surfaces and sometimes dried and rehydrated [10,18], our fibers were suspended in solution, allowing plasmin to digest from all dimensions and fibrin to both leave and

slide along the fiber during digestion. Adsorption would prevent some of the molecules from leaving the fiber and prevent the sliding of molecules along the fiber during digestion, which could explain why fibers appear to briefly “swell” during digestion in some AFM experiments [18].

The observation of fluorescence longitudinally sliding along the fiber was surprising and constitutes a previously unknown mechanism during digestion. Sliding often started slowly but became more prominent towards the end of digestion, and typically occurred as fluorescence signal moved away from digestion sites, in either direction. This sliding of signal clearly indicated that the fluorescently labeled fibrin was changing locations along the fiber. This could not be a result of plasmin digesting longitudinally down the fiber, or that would result in a loss of fluorescence, as opposed to a change in location of the fluorescence signal. Interestingly, sliding could start one direction, but then move back in another direction (left green arrow in Fig. 6A). Because there are multiple digestion sites on the fiber, this is likely the result of competing digestion sites within the fiber shifting the distribution of tension along the fiber, causing the direction of sliding to change.

The mechanisms responsible for fibrin sliding likely depend on the inherent tension present in fibrin fibers [13,15]. Fibrin fibers polymerize into a state of tension, although the exact mechanisms responsible for the fiber tension have been debated [13,19,20]. The observation of cone-shaped ends of cleaved fibers (Fig. 6C) is consistent with previously described “splayed ends” observed in EM studies of fibrinolysis [16] and indicates that protofibrils explode backward due to tension after being cut. Recent work indicates that inherent fiber tension plays a predominant role in regulating the clearance of fibrin from a region during fibrinolysis [15], and fluorescence sliding implies that tension regulates the digestion of individual fibers as well. We propose two possible mechanisms (models) that could account for tension-dependent fibrin sliding (Fig. 7).

The first model (protofibril recoil, Fig. 7A) is an analogy to a tensed rope, where, as the strands of the rope are cut, they spring backwards, leading to fiber “fraying”. Within a fiber, tensed protofibrils will also spring backwards as they are digested by plasmin, which is consistent with the observed cone-shaped fiber ends (Fig. 6C) and would lead to the appearance of fibrin sliding along the fiber. SEM images showing a registry of fibrin molecules along the fiber [19,35], along with recent polymerization and structural models [36,37], suggest that interactions between molecules along the length of the fiber would limit the extent to which a protofibril could move backwards in any single recoil event. We investigated the distance of individual sliding events between consecutive frames (Supplemental Fig. 11), but a clear trend was not present, perhaps because a frame rate of 2.5 s could not distinguish molecular scale events. If the protofibril recoil model is correct, this would constrain models of fiber tension, because sliding (recoil) occurs predominantly towards the end of digestion, and thus tension must be present in the fiber until it is fully cleaved. Models where tension originates from twisting of protofibrils around the fiber would suggest that tension is highest at thicker parts of the fiber and decreases during digestion.

The second model (molecular stretching, Fig. 7B) relies on the observation that individual fibrin molecules can unfold under force [38–41] and assumes that the tension remains relatively constant as the fiber is digested. Since inherent fiber tension is distributed throughout the cross section of a fibrin fiber, as protofibrils are cut, the tension must be redistributed among the remaining protofibrils, increasing their individual tensions. Eventually the molecular tension will be high enough (~100 pN) to unfold fibrin molecules, causing the intact molecules to begin stretching out and resulting in the longitudinal sliding of fibrin.

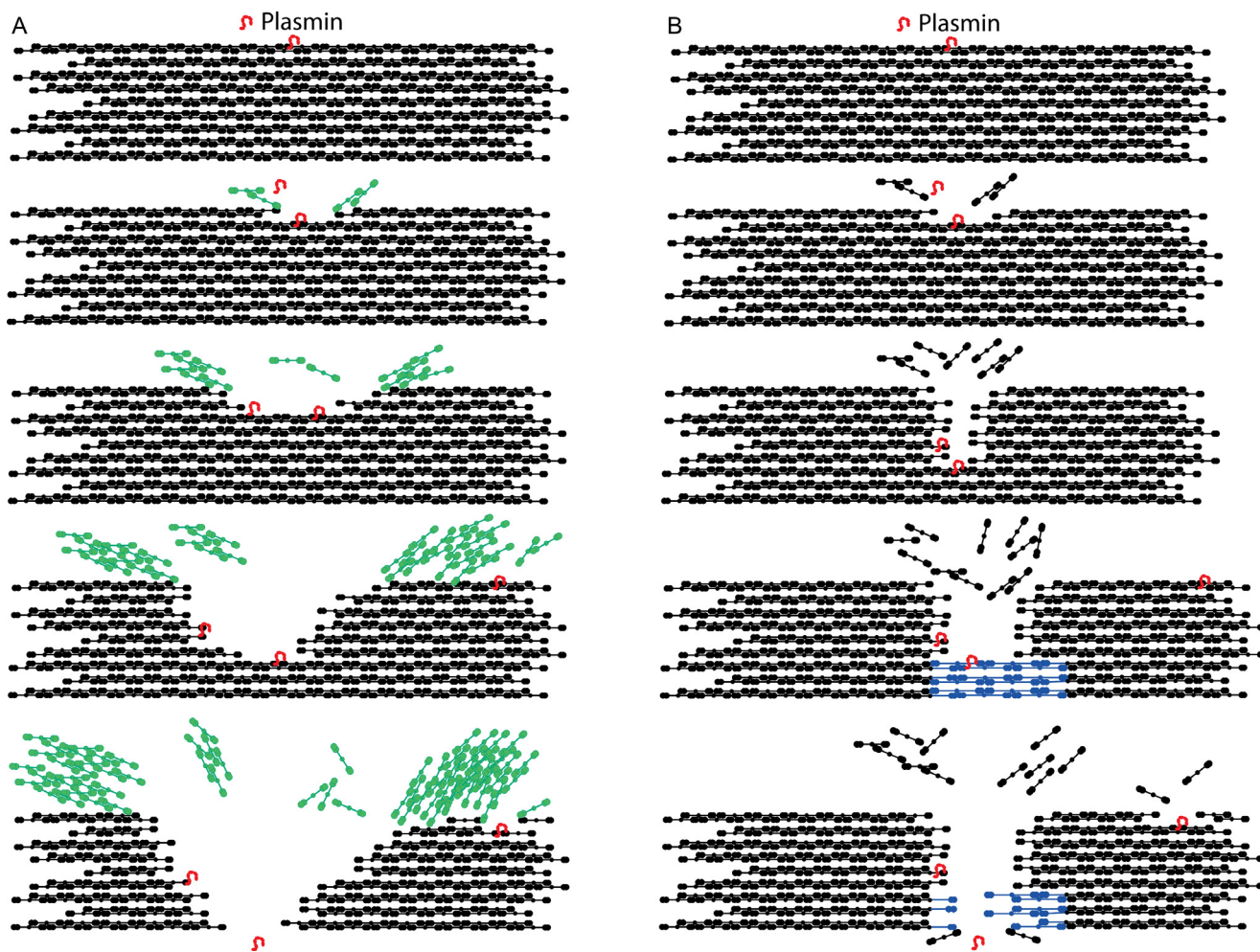


Fig. 7. Models for Single Fiber Fibrinolysis. (A) Protomembrane recoil model: Protomembranes, which are under tension in fibers, spring backwards as they are cleaved (in green), similar to how the strands of a tensed rope spring backward as they are cut. The springing backwards causes the fiber to appear as if it's being pulled apart. (B) Molecular stretching model: Protomembranes are under tension in fibers, and as protomembranes are cut, that tension is spread out across fewer and fewer protomembranes in a fiber cross section. Eventually the force on each protomembrane is enough to unfold the remaining fibrin molecules (in blue) making up the protomembranes, causing the fiber to slide apart. Here we show cut fibrin molecules leaving the fiber, rather than the protomembranes recoiling, to distinguish the mechanisms, but protomembrane recoil could also occur concurrently with the molecular stretching model shown in panel B. (For interpretation of the references to colour in this figure legend, the reader is referred to the web version of this article.)

Additional experiments are required to decipher the mechanisms of fibrin sliding and the role of tension in fiber digestion. Two ways that fibrin sliding could facilitate more rapid digestion are: (1) exposure of previously buried binding/cleavage sites to promote digestion of the remaining molecules and (2) clearance of fibrin away from transverse paths across the fiber, thereby removing adjacent binding sites which would otherwise "distract" plasmin from cutting across the fiber. The protomembrane recoil mechanism would result in both exposure and clearance while the molecular stretching mechanism would only result in the latter. It is possible that both sliding mechanisms play a role, for example in the early stages of fiber degradation, the inherent tension in fibers may cause protomembranes to recoil away from the digestion sites, while towards the end of digestion, molecular unfolding could occur.

Both our experimental and computational results suggest that a 20 μm -long fiber will have on average 14 distinct digestion sites when exposed to 10 μL of $\sim 1.43 \mu\text{M}$ plasmin solution. Additionally, model results show that at this plasmin concentration, the first plasmin molecule will bind to a fiber within the first second of the experiment, which is something that cannot be detected experimentally. The contrast between the experimental observation that sites between the fiber middle and edges have a higher probability of cleavage (Fig. 2A) and the modeling results indicat-

ing that the first plasmin molecules will randomly bind *anywhere* along the fiber suggests that there may be something about these locations that make them predisposed to being cut. Future experiments should investigate possible mechanisms for this observation. Taken together, the modeling data underscore how discretely and quickly plasmin can act and provide the most fine-scale information to-date about the timing and action of plasmin on single fiber lysis.

Furthermore, our model is the first microscale model of plasmin-fibrin interaction, and it can be used to elucidate other factors affecting fibrinolysis, e.g., the impact of plasmin binding rate (Supplement Section C.6). Studies like these can be used to suggest ideal features of future therapeutics, and when combined with experimental data, to estimate unknown physiological rates. Coordinated microscale experimental and modeling work can be a powerful tool for uncovering mechanisms of lysis that are impossible to do with experimentation or computation alone. For example, coupling our model and experimental data allowed us to estimate the amount of plasmin (0.0001% of initial amount) that immediately infiltrates the entire experimental volume when a 10 μL droplet containing plasmin is added to an existing 10 μL droplet (Supplement Section C.4). The work presented here can also be extended to study – for the first time at the scale of individual fibers

– the positive feedback mechanism by which the plasmin degradation of fibrin exposes additional binding sites for lytic enzymes [17,32,33], thereby accelerating lysis. Our single fiber approach has the potential to uncover significant new information about this positive feedback and its implications for therapeutics.

Our data also allow a careful investigation into fiber properties that may govern digestion rates. The strongest correlation we found was between the most rapid digestion site and the initially thickest part of the fiber (Fig. 4B). This is likely a consequence of the observed longitudinal sliding. When fibrin slides away from a digestion site, this will give the appearance in fluorescence data that a large amount of fibrin has digested at that location. Thus, the larger the initial intensity that slides, the larger the measured digestion rate at that location will be.

At first glance the lack of correlation between the site of most rapid digestion and the eventual cleavage site is surprising (Fig. 4A). This indicates that while the tension dependent fibrin sliding is important in fiber thinning, additional factors contribute to fiber cleavage. Digestion sites occur at all points along the fibers (Supplemental Fig. 8B). However, the cleavage sites on fibers typically occur in thinner parts of the fiber (46/60 fibers are cleaved in locations that were in the lower 50% of initial fiber thickness, Fig. 5C), but only 2/60 fiber cleavage locations were in the lowest 10% of the initial thickness. In addition, there was little correlation between the initially thickest or thinnest parts of the fiber and the cleavage site (Fig. 5A&B).

In these experiments we investigated the digestion of fibrin by plasmin, which is important given plasmin's potential use as a fibrinolytic [4]. The concentration of plasmin used ($\sim 1.43 \mu\text{M}$) was similar to physiological plasminogen concentrations (2 μM) [42]. These concentrations were chosen, in part, to optimize imaging conditions, allowing fibers to be digested over the course of ~ 1 min, enabling an observation of the lysis mechanisms while limiting the effects of photobleaching (Supplemental Fig. 10). The local concentration of plasmin next to a fiber is unknown and depends on the balance of activators and inhibitors, so 1.43 μM is reasonable.

While these experiments are an exciting first step toward a deeper understanding of mechanisms of fiber digestion, future efforts should corroborate these results under more physiological conditions. For example, initiating lysis with tPA or uPA and plasminogen would enhance our understanding of the role of plasminogen activation during digestion. Moving from a 2-D experimental lysis model of individual fibers to a 3-D fibrin mesh will also be an important future step as interactions with other fibers will influence the lysis process *in vivo* [15,30]. There are also many other plasma proteins and cells that influence clot formation and lysis whose effects on fibrin digestion could be studied using this model. For instance, $\alpha 2$ -antiplasmin and thrombin activatable fibrinolysis inhibitor (TAflla) inhibit lysis by either inhibiting plasmin or by cleaving plasmin binding sites, respectively [43]. Understanding how these inhibitors, in addition to the influence of FXIIIa crosslinking, affect microscale lysis mechanisms is important.

The mathematical model, which in its present form only allows for (un)binding and diffusion of plasmin and does not account for cleavage of fibers, can be modified to include lysis and to reflect more physiological conditions. In particular, a version of the model already exists for lysis initiated by tPA [32], and both the tPA- and plasmin-initiated lysis models can be modified to include inhibitors. Experiments and the mathematical model can be iteratively adjusted and improved to explore further mechanisms of lysis under different physiological and pathological conditions.

Pathological conditions alter fibrinolysis and are important to understand mechanistically. One particularly relevant application in light of the global COVID-19 pandemic is the observation that the SARS-CoV-2 spike protein alters clot structure and hinders fib-

rinolysis [44]. Clots from COVID patients also contain "microclots" with increased $\alpha 2$ -antiplasmin and amyloid deposits [45]. Fibrinogen and/or fibrin have been shown to participate in amyloid formation with other proteins including β -amyloid in Alzheimer's disease [46,47], serum amyloid A [48], and amylin fibrils in type 2 diabetes [49], often leading to hindered fibrinolysis, perhaps due to decreased binding of plasmin(ogen) [46] or altered clot structures. Fibrin has also been shown to form "plate" or "sheet" [20] structures, the presence of which are increased under amyloidogenic conditions [50]. The experimental approaches described herein could help to uncover the mechanisms responsible for aberrant lysis in many of these disorders by observing fiber digestion in conditions mimicking these pathological situations. We hypothesize that in amyloidic fibrin fibers, the fibrin sliding mechanism may be altered due to amyloid β -sheet structures locking fibrin molecules into place.

We conclude that studying the lysis of individual fibers reveals previously undiscovered mechanisms of fiber digestion. Fiber lysis is a balance of digestion by plasmin and tension-dependent fibrin sliding. The presence of fibrin sliding was an unexpected mechanism and adds to the growing body of evidence that inherent fiber tension plays important roles in regulating fibrinolysis [15]. The digestion mechanisms revealed in these studies provide a new framework for future biochemical and clinical studies investigating factors that alter blood clot digestion. This, in turn, will help to unravel the mystery of why up to 20% of clots are resistant to thrombolytic treatments [6] and inform the development of next-generation therapeutics.

Declaration of Competing Interest

The authors declare that they have no known competing financial interests or personal relationships that could have appeared to influence the work reported in this paper.

Acknowledgments

NEH gratefully acknowledges support by Grant Number HL148842. The content of this work is solely the responsibility of the authors and does not necessarily represent the official views of the NHLBI or NIH. BEB and SML gratefully acknowledge support from the University of Central Oklahoma College of Mathematics and Science CURE-STEM award. SRL gratefully acknowledges support from the ECU URCA and UR Mini awards.

Supplementary materials

Supplementary material associated with this article can be found, in the online version, at doi:[10.1016/j.actbio.2022.01.006](https://doi.org/10.1016/j.actbio.2022.01.006).

Reference

- [1] S.S. Virani, A. Alonso, H.J. Aparicio, E.J. Benjamin, M.S. Bittencourt, C.W. Callaway, A.P. Carson, A.M. Chamberlain, S. Cheng, F.N. Delling, M.S.V. Elkind, K.R. Evenson, J.F. Ferguson, D.K. Gupta, S.S. Khan, B.M. Kissela, K.L. Knutson, C.D. Lee, T.T. Lewis, J. Liu, M.S. Loop, P.L. Lutsey, J. Ma, J. Mackey, S.S. Martin, D.B. Matchar, M.E. Mussolini, S.D. Navaneethan, A.M. Perak, G.A. Roth, Z. Samad, G.M. Satou, E.B. Schroeder, S.H. Shah, C.M. Shay, A. Stokes, L.B. Van-Wagner, N. Wang, C.W. Tsao, Heart disease and stroke statistics-2021 update: a report from the American Heart Association, *Circulation* 143 (2021) e254–e743.
- [2] N.E. Hudson, in: *Biophysical Mechanisms Mediating Fibrin Fiber Lysis*, BioMed Research International, 2017, p. 2017.
- [3] Tissue Plasminogen Activator for Acute Ischemic Stroke (Alteplase, Activase®).
- [4] P.J. Mitchell, et al., Plasmin (Human) administration in acute middle cerebral artery ischemic stroke: phase 1/2a, open-label, dose-escalation, safety study, *J. Stroke Cerebrovasc. Dis.* 26 (2017) 308–320.
- [5] X. Liu, Beyond the time window of intravenous thrombolysis: standing by or by stenting? *Interv. Neurol.* 1 (2012) 3–15.
- [6] C. Kluft, J.J. Sidemann, J.B. Gram, Assessing safety of thrombolytic therapy, *Semin. Thromb. Hemost.* 43 (3) (2017) 300–310, doi:[10.1055/s-0036-1584130](https://doi.org/10.1055/s-0036-1584130).

- [7] S.M. Wolpert, H. Bruckmann, R. Greenlee, L. Wechsler, M.S. Pessin, G.J. Del Zoppo, Neuroradiologic evaluation of patients with acute stroke treated with recombinant tissue plasminogen activator, *Am. J. Neuroradiol. AJNR* 14 (1993) 3–13.
- [8] W.J.G. Schielen, M. Voskuilen, G.I. Tesser, W. Nieuwenhuizen, The sequence Aα-(148–160) in fibrin, but not in fibrinogen, is accessible to monoclonal antibodies, *Proc. Natl. Acad. Sci. U. S. A.* 86 (1989) 8951–8954.
- [9] W.J. Schielen, H.P. Adams, K. van Leuven, M. Voskuilen, G.I. Tesser, W. Nieuwenhuizen, The sequence gamma-(312–324) is a fibrin-specific epitope, *Blood* 77 (1991) 2169–2173.
- [10] A. Blinc, J. Magdic, J. Fric, I. Musevic, Atomic force microscopy of fibrin networks and plasma clots during fibrinolysis, *Fibrinolysis Proteolysis* 14 (2000) 288–299.
- [11] S.L. Diamond, S. Anand, Inner clot diffusion and permeation during fibrinolysis, *Biophys. J.* 65 (1993) 2622–2643.
- [12] D.A. Gabriel, K. Muga, E.M. Boothroyd, The effect of fibrin structure on fibrinolysis, *J. Biol. Chem.* 267 (1992) 24259–24263.
- [13] I. Bucay, O.E. Tim, S.D. Wulfe, R. Superfine, A.S. Wolberg, M.R. Falvo, N.E. Hudson, Physical determinants of fibrinolysis in single fibrin fibers, *PLoS One* 10 (2015) e0116350.
- [14] J. Collet, C. Lesty, G. Montalescot, J.W. Weisel, Dynamic changes of fibrin architecture during fibrin formation and intrinsic fibrinolysis of fibrin-rich clots, *J. Biol. Chem.* 278 (2003) 21331–21335.
- [15] S.J. Cone, A.T. Fuquay, J.M. Lifovsky, T.C. Dement, C.A. Carolan, N.E. Hudson, Inherent fibrin fiber tension propels mechanisms of network clearance during fibrinolysis, *Acta Biomater.* 107 (2020) 164–177.
- [16] Y. Veklich, C.W. Francis, J. White, J.W. Weisel, Structural studies of fibrinolysis by electron microscopy, *Blood* 92 (1998) 4721.
- [17] J. Weisel, R. Litvinov, The biochemical and physical process of fibrinolysis and effects of clot structure and stability on the lysis rate, *Cardiovasc. Hematol. Agents Med. Chem.* 6 (2008) 161–180.
- [18] T. Feller, J. Hársfalvi, C. Csányi, B. Kiss, M. Kellermayer, Plasmin-driven fibrinolysis in a quasi-two-dimensional nanoscale fibrin matrix, *J. Struct. Biol.* 203 (2018) 273–280.
- [19] J.W. Weisel, C. Nagaswami, L. Makowski, Twisting of fibrin fibers limits their radial growth, *Proc. Natl. Acad. Sci. U. S. A.* 84 (1987) 8991–8995.
- [20] E.T. O'Brien, M.R. Falvo, D. Millard, B. Eastwood, R.M. Taylor, R. Superfine, Ultrathin self-assembled fibrin sheets, *Proc. Natl. Acad. Sci. U. S. A.* 105 (2008) 19438–19443.
- [21] S.R. Sternberg, in: *Biomedical Image Processing*, 16, IEEE Computer, 1983, pp. 22–34.
- [22] J. Schindelin, I. Arganda-Carreras, E. Frise, V. Kaynig, M. Longair, T. Pietzsch, S. Preibisch, C. Rueden, S. Saalfeld, B. Schmid, J. Tinevez, D.J. White, V. Hartenstein, K. Eliceiri, P. Tomancak, A. Cardona, Fiji: an open-source platform for biological-image analysis, *Nat. Methods* 9 (2012) 676–682.
- [23] W. Li, J. Sigley, S.R. Baker, C.C. Helms, M.T. Kinney, M. Pieters, P.H. Brubaker, R. Cubicotti, M. Guthold, Nonuniform internal structure of fibrin fibers: protein density and bond density strongly decrease with increasing diameter, *BioMed Res. Int.* 2017 (2017) 6385628–13, doi:10.1155/2017/6385628.
- [24] D.T. Gillespie, A. Hellander, L.R. Petzold, Perspective: stochastic algorithms for chemical kinetics, *J. Chem. Phys.* 138 (17) (2013) 170901, doi:10.1063/1.4801941.
- [25] S.A. Isaacson, C.S. Peskin, Incorporating diffusion in complex geometries into stochastic chemical kinetics simulations, *SIAM J. Sci. Comput.* 28 (2006) 47–74.
- [26] R. Erban, S.J. Chapman, *Stochastic Modelling of Reaction-Diffusion Processes*, Cambridge University Press, Cambridge, 2019.
- [27] The R Core Team, R: a language and environment for statistical computing, R foundation for statistical computing, (2021).
- [28] N.F. Polizzi, M.J. Therien, D.N. Beratan, Mean first-passage times in biology, *Isr. J. Chem.* 56 (2016) 816–824.
- [29] S. Iyer-Biswas, A. Zilman, First-passage processes in cellular biology, in: *Anonymous Advances in Chemical Physics*, John Wiley & Sons, Inc, Hoboken, NJ, 2016, pp. 261–306.
- [30] J. Collet, D. Park, C. Lesty, J. Soria, C. Soria, G. Montalescot, J. Weisel, Influence of fibrin network conformation and fibrin fiber diameter on fibrinolysis speed: dynamic and structural approaches by confocal microscopy, arteriosclerosis, thrombosis, and vascular biology, *J. Am. Heart Assoc.* 20 (2000) 1354–1361.
- [31] D.V. Sakharov, D.C. Rijken, Superficial accumulation of plasminogen during plasma clot lysis, *Circulation* 92 (1995) 1883–1890.
- [32] B.E. Bannish, I.N. Chernysh, J.P. Keener, A.L. Fogelson, J.W. Weisel, Molecular and physical mechanisms of fibrinolysis and thrombolysis from mathematical modeling and experiments, *Sci. Rep.* 7 (2017) 6914–11.
- [33] J.W. Weisel, Y. Veklich, J.P. Collet, C.W. Francis, Structural studies of fibrinolysis by electron and light microscopy, *Thromb. Haemost.* 82 (1999) 277–282.
- [34] W. Li, R. Li, T. Lucioni, K. Bonin, S.S. Cho, M. Guthold, Stretching single fibrin fibers hampers their lysis, *Acta Biomater.* 60 (2017) 264–274.
- [35] W.A. Voter, C. Lucaveche, A.E. Blaurock, H.P. Erickson, Lateral packing of protofibrils in fibrin fibers and fibrinogen polymers, *Biopolymers* 25 (1986) 2359–2373.
- [36] M. Rocco, M. Molteni, M. Ponassi, G. Giachi, M. Frediani, A. Koutsoubas, A. Profumo, D. Trevorin, B. Cardinali, P. Vachette, F. Ferri, J. Pérez, A comprehensive mechanism of fibrin network formation involving early branching and delayed single- to double-strand transition from coupled time-resolved X-ray/light-scattering detection, *J. Am. Chem. Soc.* 136 (2014) 5376.
- [37] O. Klykov, C. van der Zwaan, A.J.R. Heck, A.B. Meijer, R.A. Scheltema, Missing regions within the molecular architecture of human fibrin clots structurally resolved by XL-MS and integrative structural modeling, *Proc. Natl. Acad. Sci. PNAS* 117 (2020) 1976–1987.
- [38] A. Zhmurov, A.X. Brown, R. Litvinov, R. Dima, J. Weisel, V. Barsegov, Mechanism of fibrin(ogen) forced unfolding, *Structure* 19 (2011) 1615–1624.
- [39] L.E. Averett, M.H. Schoenfisch, B.B. Akhremitchev, O.V. Gorkun, Kinetics of the multistep rupture of fibrin 'A'- polymerization interactions measured using atomic force microscopy, *Biophys. J.* 97 (2009) 2820–2828.
- [40] A.X. Brown, R.I. Litvinov, D.E. Discher, J.W. Weisel, Forced unfolding of coiled-coils in fibrinogen by single-molecule AFM, *Biophys. J.* 92 (2007) L39–L41.
- [41] N.E. Hudson, F. Ding, I. Bucay, E.T. O'Brien, O.V. Gorkun, R. Superfine, S.T. Lord, N.V. Dokholyan, M.R. Falvo, Submillisecond elastic recoil reveals molecular origins of fibrin fiber mechanics, *Biophys. J.* 104 (2013) 2671–2680.
- [42] D. Collen, G. Tytgat, H. Claeys, M. Verstraete, P. Wallén, Metabolism of plasminogen in healthy subjects: effect of tranexamic acid, *J. Clin. Invest.* 51 (1972) 1310–1318.
- [43] B.E. Bannish, N.E. Hudson, The utility and potential of mathematical models in predicting fibrinolytic outcomes, *Curr. Opin. Biomed. Eng.* 20 (2021) 100337.
- [44] L. Grobbelaar, C. Venter, M. Vlok, M. Ngoepe, G. Laubscher, P. Lourens, J. Steenkamp, D. Kell, E. Pretorius, SARS-CoV-2 spike protein S1 induces fibrin(ogen) resistant to fibrinolysis: implications for microclot formation in COVID-19, *Biosci. Rep.* 41 (2021).
- [45] E. Pretorius, M. Vlok, C. Venter, J.A. Bezuidenhout, G.J. Laubscher, J. Steenkamp, D.B. Kell, Persistent clotting protein pathology in long COVID/Post-acute sequelae of COVID-19 (PASC) is accompanied by increased levels of antiplasmin, *Cardiovasc. Diabetol.* 20 (2021) 1–172.
- [46] D. Zamolodchikov, S. Strickland, $\text{A}\beta$ delays fibrin clot lysis by altering fibrin structure and attenuating plasminogen binding to fibrin, *Blood* 119 (2012) 3342–3351.
- [47] M. Cortes-Canteli, J. Paul, E.H. Norris, R. Bronstein, H.J. Ahn, D. Zamolodchikov, S. Bhuvanendran, K.M. Fenz, S. Strickland, Fibrinogen and β -amyloid association alters thrombosis and fibrinolysis: a possible contributing factor to Alzheimer's disease, *Neuron* 66 (2010) 695–709 (Cambridge, Mass.).
- [48] M.J. Page, G.J.A. Thomson, J.M. Nunes, A. Engelbrecht, T.A. Nell de Villiers, J.S. Willem, M.C. de Beer, L. Engelbrecht, D.B. Kell, E. Pretorius, Serum amyloid A binds to fibrin(ogen), promoting fibrin amyloid formation, *Sci. Rep.* 9 (2019) 3102.
- [49] E. Pretorius, S. Mbotwe, D.B. Kell, Lipopolysaccharide-binding protein (LBP) reverses the amyloid state of fibrin seen in plasma of type 2 diabetics with cardiovascular co-morbidities, *Sci. Rep.* 7 (2017) 9680–16.
- [50] E. Pretorius, S. Mbotwe, J. Bester, C.J. Robinson, D.B. Kell, Acute induction of anomalous and amyloidogenic blood clotting by molecular amplification of highly substoichiometric levels of bacterial lipopolysaccharide, *J. R. Soc. Interface* 13 (2016) 20160539.

Microscale Structural Changes of Individual Fibrin Fibers During Fibrinolysis

Spencer R. Lynch¹, Sean M. Laverty², Brittany E. Bannish², Nathan E. Hudson¹

¹Dept. of Physics, East Carolina University, Greenville, NC, USA.

-spencerlynch320@gmail.com, hudsonn16@ecu.edu

²Dept. of Mathematics and Statistics, University of Central Oklahoma, Edmond, OK, USA.

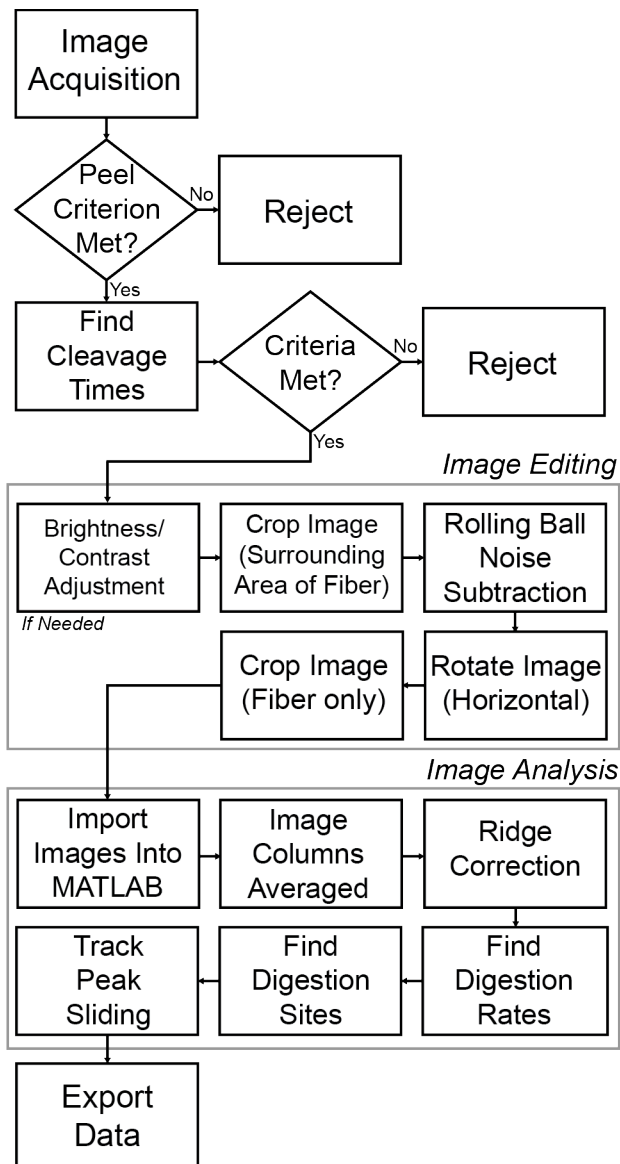
-slaverty@uco.edu, bbannish@uco.edu

Supplemental Data and Information

A. Materials and Methods

A.1 Sample Preparation

The labeled (Alexa Fluor™ 488 conjugate, pH 8.3, Invitrogen by Thermo Fisher Scientific/Life Technologies Corporation, Eugene, OR) and unlabeled (Peak 1, pH 7.4, Enzyme Research Labs (ERL), Indianapolis, IN) fibrinogen concentrations (0.0308 mg/mL and 2.0 mg/mL), respectively correspond to a 1:65 (Alexa488 labeled fibrinogen: unlabeled fibrinogen) ratio, which was chosen to optimize fluorescent signal without compromising fibrin polymerization. Aliquots (25 U/mL) of human alpha thrombin (ERL) were thawed from -80.0 °C and diluted to 0.2 U/mL using 10mM CaCl₂ in HBS and mixed in equal volume with fibrinogen (10 μL each) on the ridged surface giving a final fibrinogen concentration of 1 mg/mL, and thrombin at 0.1 U/mL. The samples were polymerized for one hour at 37 °C. Samples were then gently pipetted to remove outer fibrin gel layers, leaving fibrin fibers near the micropatterned surface before 10 μL of HBS was returned. Plasmin aliquots (ERL, 2 U/mL) were thawed from -20.0°C and diluted to 0.132 U/mL using 10mM CaCl₂ HBS buffer and 10 μL of the resulting solution was added to polymerized fibrinogen samples on the microscope, bringing final volume and plasmin concentration to 20 μL and 0.066 U/mL.



Supplemental Figure 1: Analysis Pipeline. This figure shows how experimental data was extracted from acquired images. The “Criteria Met?” decision junction refers to whether the fiber met all other criteria laid out in A.4.

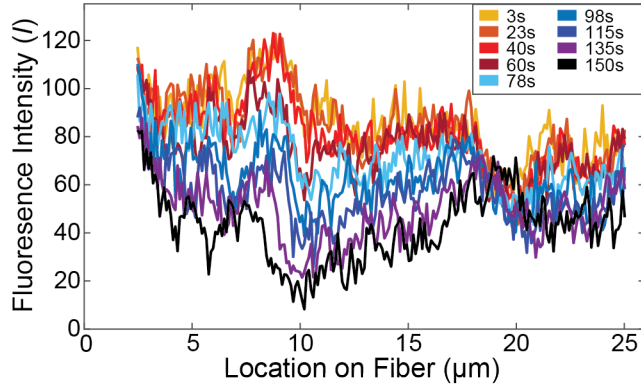
A.2 Contrast and Brightness Adjustment

For ~35% of fibers the contrast and brightness were adjusted using FIJI/ImageJ’s [1,2] auto brightness and contrast function as acquisition software sometimes returned dark images. Tests showed adjusting brightness and contrast improved fiber visualization, but did not alter normalized intensities, digestion rates, the number of digestion sites, etc. (all described below), and thus the brightness/contrast enhancement did not influence any of the results.

A.3 Intensity Profiles

To investigate the fluorescence intensity at every location along the length of the fiber, we created a plot of the average cross-sectional intensity vs location. This will be

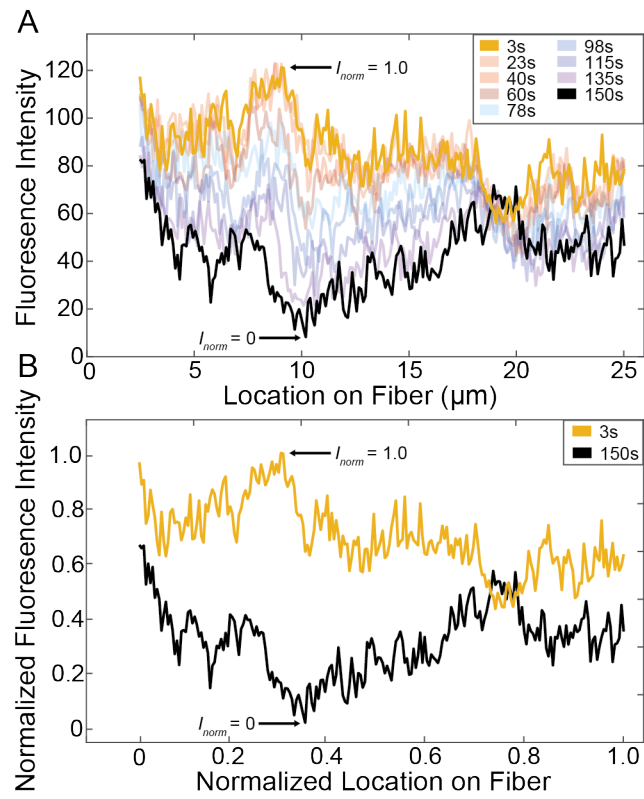
referred to as a cross-sectional intensity profile. To study how the intensity profiles change over time, we divided the time series into eight equally-spaced timepoints plus the final timepoint before cleavage and plotted each of the nine intensity profiles. A representative plot is shown in Supplemental Figure 2. As can be observed, the cross-sectional intensity is non-uniform along the length of the fiber at any given timepoint, and the cross-sectional intensity decreases over time at most locations. This was consistent among all fibers studied.



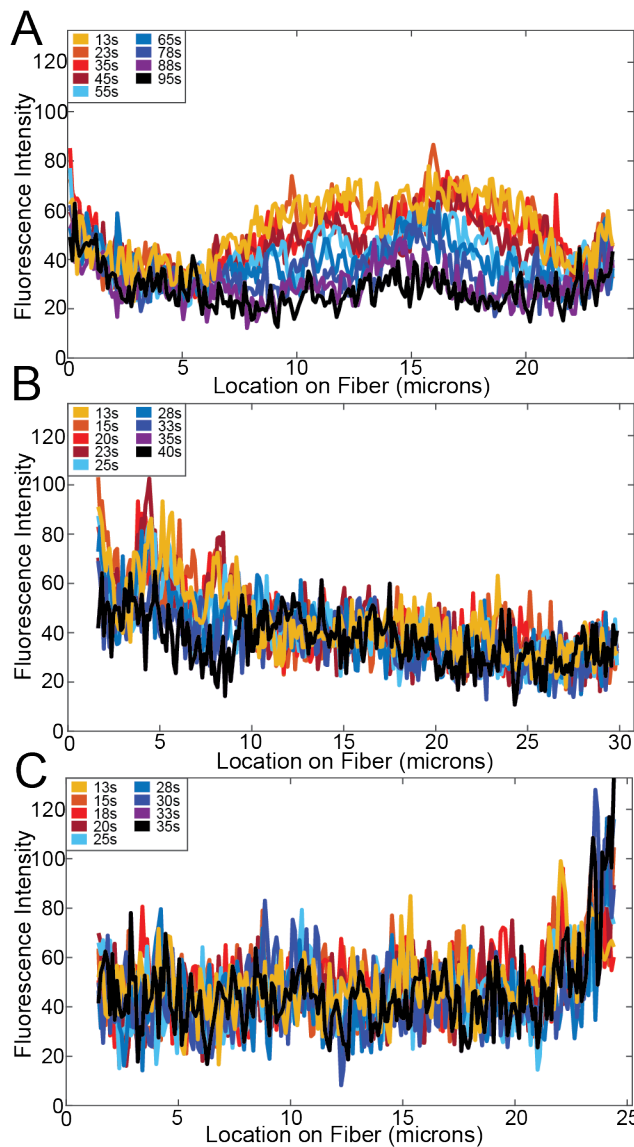
Supplemental Figure 2: Cross-Sectional Intensity Profiles for Multiple Instances in Time.
Plots of the average cross-sectional intensity versus location along the fiber at nine different time points during digestion for a representative fiber.

A.4 Inclusion/Exclusion Criteria

Fibers that peeled from the ridges (as opposed to being cleaved) (71 total), were connected to other fibers via branch points, or had their midpoint shift vertically (perpendicular to fiber length) by more than $0.5\text{ }\mu\text{m}$ were excluded from analysis because each of these features created aberrations in the fluorescence-based digestion rates (69 total). Lysis times were collected for all fibers that did not peel (178 total) from the ridges as the other criteria played no role in their analysis. Image series with a poor digestion signal ratio (showing very little change in transverse intensity during digestion) were not included in the digestion rate data analysis. An image series' digestion signal ratio was calculated by first normalizing the fiber's first and last intensity profile, from the first and last image of a time series, by setting the maximum of the first profile to 1 and the minimum of the last profile to 0. Then the average of the normalized intensity profile for the first frame was divided by the average of the normalized intensity profile for the last frame to calculate the digestion signal ratio (Supplemental Figure 3). The digestion signal ratio represents how much larger the changes in fluorescence signal due to digestion are than changes in fluorescent signal due to noise. The digestion signal ratio was calculated for every fiber and fibers were manually segregated by comparing locations of bright and dim fiber spots with the corresponding cross-sectional fluorescence signal. We found that fibers with digestion signal ratios lower than 5.2 had poor correspondence between bright fiber spots and cross-sectional fluorescence values because the noise around the edges of fibers could drown out fiber signal. So, every fiber with a digestion signal ratio less than 5.2 was excluded from analysis, eliminating an additional 46 fibers, leaving a total of 60 fibers for this analysis. Intensity profiles for three fibers with three different digestion signal ratios are shown in Supplemental Figure 4.



Supplemental Figure 3: Intensity Normalization for Exclusion Criteria. A) Plot showing cross-sectional intensity profiles with the first (gold) and last (black) profiles of the time series highlighted in bold. B) Same plot as in A), but with normalized fluorescence intensity (I_{norm}) values and showing only the first (gold) and last (black) intensity profiles of the time series. In both plots the maximum of the first profile and the minimum of the last profile are indicated.

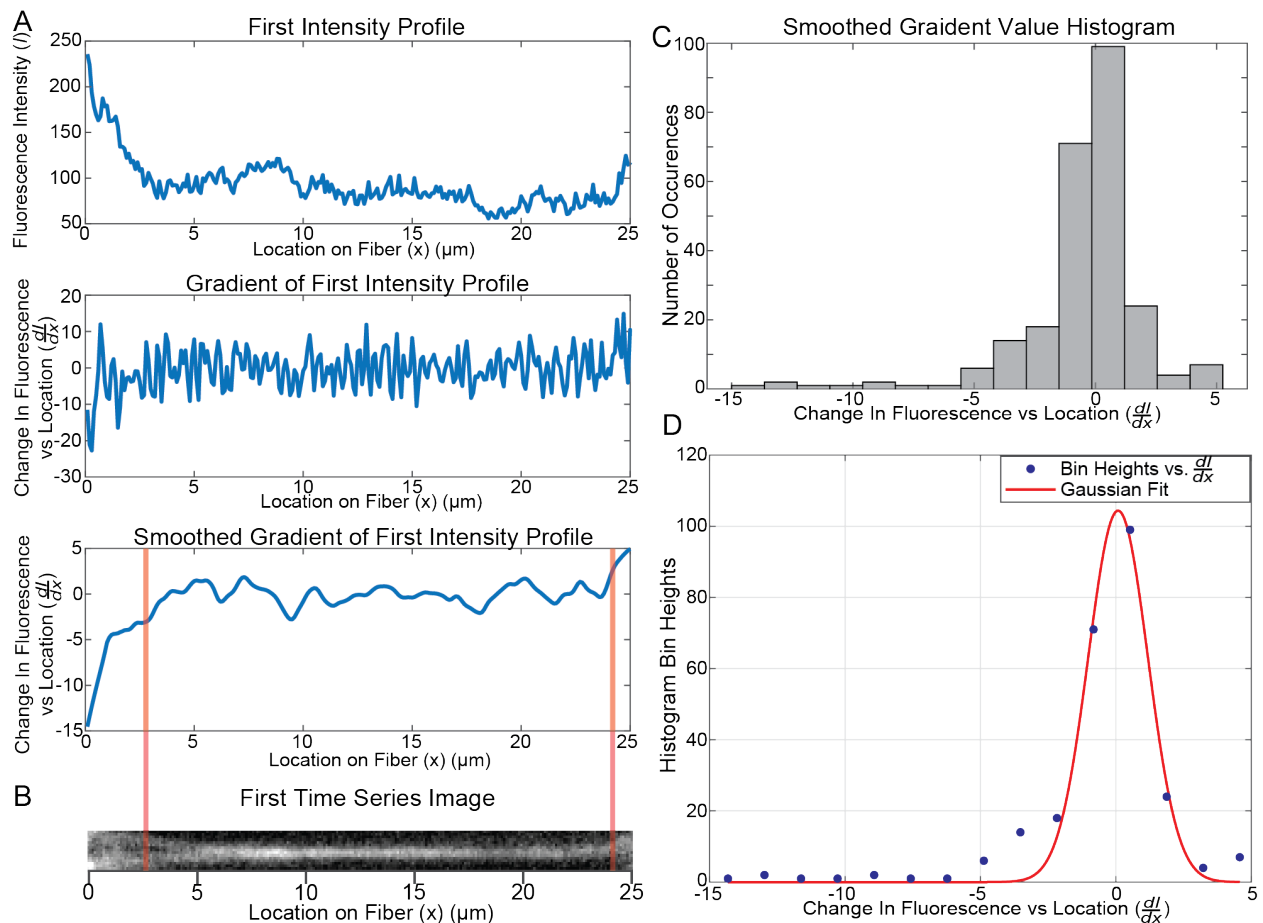


Supplemental Figure 4: Digestion Signal Ratio for Exclusion Criteria. Plots of the cross-sectional intensity profiles at nine different time points during digestion for three different fibers of differing amounts of noise. A) Plot showing a digestion signal ratio of 29.5. B) Plot showing a digestion signal ratio of 6.9. C) Plot showing a digestion signal ratio of 4.7 (below the 5.2 cutoff).

A.5 Fiber End Trimming

Because fibers were polymerized between ridges, the ends of fibers often were brighter due to ridge autofluorescence. To avoid including autofluorescence signal in the cross-sectional intensity profiles, the ends of the fiber were not considered during analysis. Fiber ends were trimmed as part of the analysis algorithm pipeline (Supplemental Figure 1) using the following protocol. On the first image in the time series, the MATLAB “gradient” function was used to find the change in average longitudinal fluorescence intensity with respect to location at every location along the fiber (Supplemental Figure 5A). The intensity gradient was smoothed using the built-in MATLAB “smooth” function, with the “rlowess” algorithm with a smoothing parameter of 18 (Supplemental Figure 5A). Using MATLAB’s built in “histogram” and “fit” functions, a

15-bin histogram was made of the smoothed gradient at each location along the fiber and a Gaussian curve was fit to the data (Supplemental Figure 5C&D). Analyzing data fits from ten randomly selected fibers, we determined that if the smoothed gradient value was greater than two standard deviations higher than the mean, this likely originated from ridge autofluorescence. Thus, we removed contiguous sections of fiber ends with smoothed gradient values greater than two standard deviations (Supplemental Figure 5B). This resulted in 2.85 μm , on average, being cut from the fiber. For the 35% of timeseries with high intensity values, a two standard deviation cutoff still left autofluorescence signal, so higher cutoff values were selected by iteratively increasing the threshold until the ends of the smoothed gradient plot (Supplemental Figure 5A) were within the bounds of the smoothed gradient values measured at locations in the middle of the fiber.

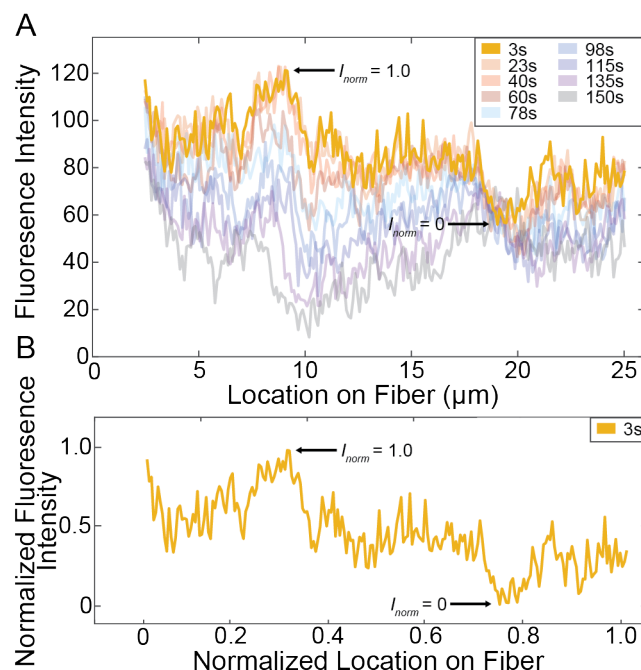


Supplemental Figure 5: Fiber End Trimming Algorithm. A) Plots showing the first intensity profile of the time series (top), the gradient of the first intensity profile (middle), and the smoothed gradient of the first intensity profile (bottom) for the fiber in panel B. B) Representative fiber image showing the approximate location where the fiber ends would be trimmed. C) Histogram of smoothed gradient values from the bottom plot of A. D) Plot of the bin heights from panel C with a Gaussian curve fit to the data.

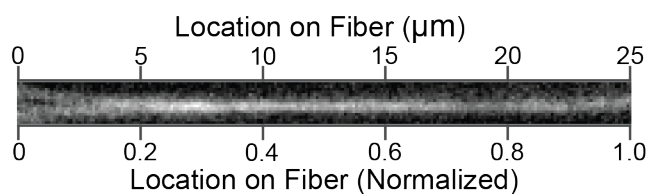
A.6 Length and Intensity Normalization

Fibers have different raw intensity values based on the number of fluorescent molecules present, fiber thickness, camera settings, etc., so no quantitative trends can be deduced from raw intensity data. However, we can look for trends between fibers by using normalized intensity data relative to the fiber's brightest and dimmest spots. Specifically, at each location along the fiber we subtracted the minimum initial cross-sectional intensity value, thereby setting the dimmest location along the fiber to have a cross-sectional intensity value of zero. We then divided each value by the new maximum initial cross-sectional intensity value, thereby normalizing the initial cross-sectional intensities values, with the brightest spot having a normalized intensity value of 1 (Supplemental Figure 6).

In addition, because fibers have different lengths, we normalized locations along the fiber. This was done by setting the left most location on fibers to zero and dividing the length at each location on the fiber by the total fiber length, thereby giving the right most location a normalized length of one and all locations between the ends normalized lengths between zero and one (Supplemental Figure 7).



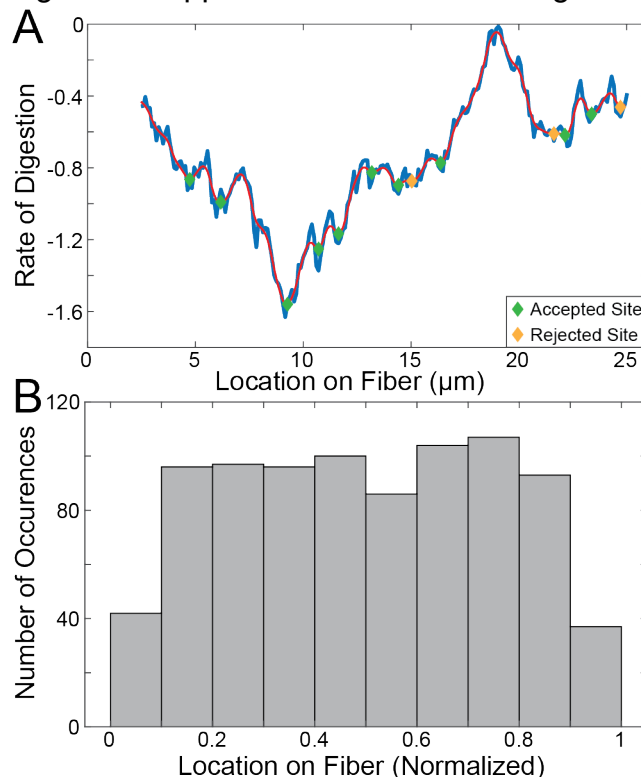
Supplemental Figure 6: Intensity Normalization for Fiber Comparison. A) Plot showing intensity profiles with the first profile (gold) of the timeseries highlighted. B) Normalized plot showing only the first intensity profile of the timeseries. In both plots the maximum (normalized intensity = 1.0) and minimum (normalized intensity = 0) of the first intensity profile is indicated.



Supplemental Figure 7: Length Normalization. A micrograph of a representative fiber with top axis showing the location on the fiber in microns and bottom axis showing the location on the fiber after the location has been normalized.

A.7 Digestion Site Prominence Criteria

To identify digestion site locations, a spline was fit to the rate of digestion profile and local minima of the fit function were identified using MATLAB's "islocalmin" function, which returned the local minima locations and prominence values. A minimum's prominence value depends on its depth relative to, and its horizontal distance from, adjacent or other local minima. If the returned prominence values were less than the cutoff threshold value (0.023) then the analysis pipeline algorithm excluded them from the final data as false positives (Supplemental Figure 8A). This cutoff value was determined by taking a random selection of fibers and manually identifying local minima (corresponding to digestion sites) based on visual inspection of their prominence. The cutoff criteria prominence threshold was then specified such that the algorithm would reject the same number of minima that were manually rejected by visual inspection for the same randomly chosen sample of fibers. A histogram of every normalized digestion site shows that digestion happens at all locations along a fiber (Supplemental Figure 8B).



Supplemental Figure 8: Rate of Digestion Curve Shows Digestion Sites. A) Plot showing the rate of change of fluorescence intensity at every location along the fiber (blue), and the spline fit to the data (red). Minima meeting criteria are marked by green diamonds and rejected minima are marked by yellow diamonds. B) Histogram of locations of digestion sites from all 60 fibers. The locations are normalized as described in Supplemental Figure 7.

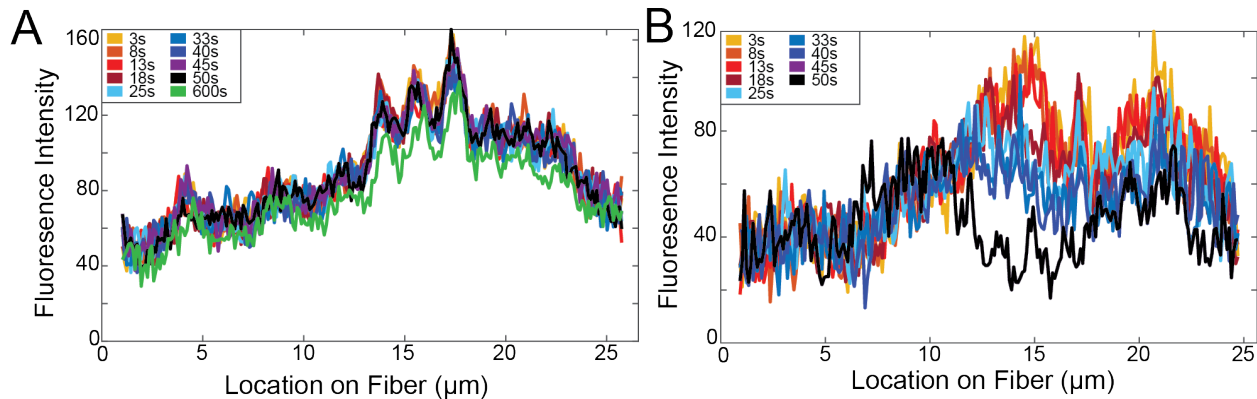
A.8 Longitudinal Fluorescence Peak Sliding

Qualitatively, videos of fiber digestion show fibers being pulled apart, with fluorescence signal sliding longitudinally away from sites of fiber digestion (Supplemental Movies). To quantify this, a spline was fit to the cross-sectional intensity profiles of the last nine frames of each fiber's digestion using the MATLAB "createfit" function. The location and height of peaks in the spline fit were then detected using the built in MATLAB "findpeaks" function. We identified 95 distinct peaks in 45 fibers whose location could be tracked throughout the duration of the timeseries (15/60 fibers had peaks that could not be assigned throughout the timeseries duration and were thus excluded from the peak sliding analysis). For each peak, the change in location between each of the frames and the total change in location between the beginning and end of the nine frames were quantified.

B. Supplemental Data

B.1 Photobleaching

To investigate the influence of photobleaching on our digestion rate calculations, we performed control experiments where we imaged fibers under identical conditions as normal experiments, except plasmin was never added. Data from a representative control experiment is shown in Supplemental Figure 9A. Because the shutter is only open when image acquisition is occurring, the light dosage is limited to only those times. Thus, for example, the fiber in Supplemental Figure 9A underwent 48.24 seconds of light exposure over a 10-minute period. When plasmin is added, fibers digest in under two minutes, so fibers used in final analysis were exposed to 4.64 seconds of light over 58.0 seconds, on average. Supplemental Figure 9A shows a nearly uniform loss of average cross-sectional intensity along the entire length of the fiber, which is dramatically different from the non-uniform loss of intensity observed when plasmin is added (example data shown in Supplemental Figure 9B). Moreover, the reduction in fluorescence intensity between control and plasmin samples is dramatic. In photobleaching controls, the last intensity profile (green curve, supplemental figure 10A) had 14% less intensity than the first intensity profile after being exposed to over 10x the light a normal fiber undergoes in our lysis experiments. Digested fibers lose 28% intensity on average in 10x less time showing that fluorescence loss from photobleaching is insignificant. Finally, the rate of intensity loss was an order of magnitude lower in control samples than in plasmin-added samples. Thus, we can conclude that photobleaching plays a very minimal role in the measured fluorescence-intensity-based plasmin digestion rates.



Supplemental Figure 9: Photobleaching Effects on Intensity Profiles. A) Plot showing the intensity profiles at nine points in time for a representative fiber that only underwent photobleaching. Note that very little intensity change occurs during the first 50 s. A much longer timepoint (600 s) is shown in green for comparison. B) Plot showing intensity profiles at nine points in time for a representative fiber that underwent plasmin digestion.

B.2 Confidence Intervals

Pearson coefficients (r) and confidence intervals were found using Minitab's (Minitab Ltd, Coventry, United Kingdom) "correlation" tool under basic statistics using a confidence value of 95%.

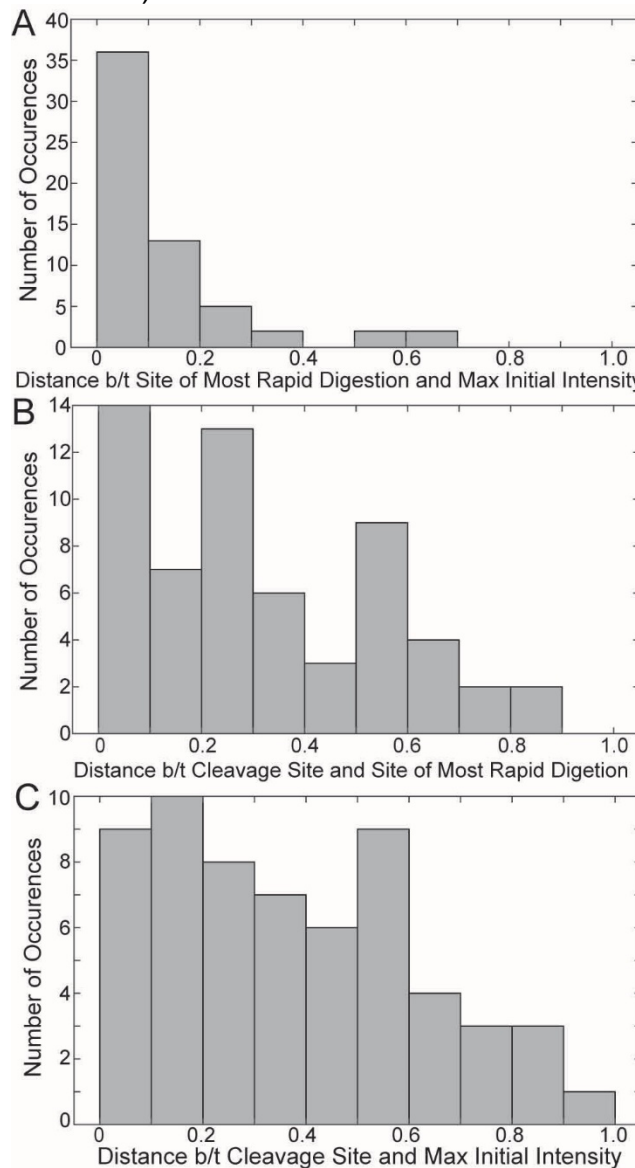
Correlation	95% Confidence Interval	Native Figure
Site of Most Rapid Digestion vs. Cleavage Site	CI = (-0.346, 0.157)	4A
Site of Most Rapid Digestion vs. Max Initial Intensity Location	CI = (0.566, 0.821)	4B
Site of Most Rapid Digestion vs. Min Initial Intensity Location	CI = (-0.644, -0.241)	4C
Max Initial Intensity Location vs. Cleavage Site	CI = (-0.473, -0.006)	5A
Min Initial Intensity Location vs. Cleavage Site	CI = (-0.071, 0.420)	5B

Supplemental Table 1: Confidence intervals for correlation analysis. The confidence intervals for each correlation, found with a significance value of 0.05, are shown.

B.3 Additional Relationships Between Fiber Properties, Digestion Rates, and Cleavage Sites

Because of the strong correlation between the location of the most rapid digestion site and the site of maximum initial intensity (Figure 4B), we further investigated this

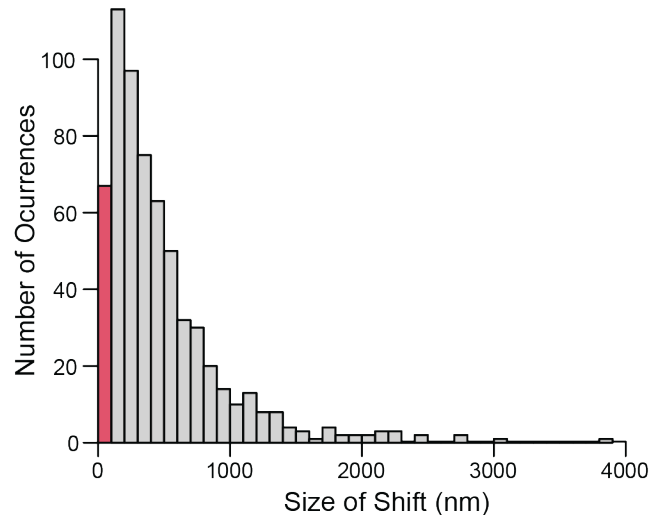
relationship by looking at the normalized distance between them. Supplemental Figure 10A shows that the majority of fibers had a most rapid digestion site and maximum initial intensity site that were within 10% of each other in normalized location. Recall the strong correlation between these sites (Figure 4B from main text). Supplemental Figure 10B shows a weak skew towards the site of most rapid digestion being near the cleavage site. Recall the weak correlation between these sites (Figure 4A from main text). Supplemental Figure 10C shows little to no skew towards the cleavage site being near the site of initial maximum intensity. Recall the lack of correlation between these two sites (Figure 5A from main text).



Supplemental Figure 10: Histograms of Distances Between Important Fiber Locations. A) Histogram showing the normalized distance between the site of most rapid digestion and the location of initial maximum intensity. B) Histogram showing the normalized distances between the cleavage site and the site of most rapid digestion. C) Histogram showing the normalized distance between the cleavage site and the location of maximum initial intensity.

B.4 Individual Step Sizes During Fluorescence Sliding

To further investigate fluorescence sliding (Figure 6), we created a histogram of the absolute value of all the individual fluorescence sliding steps. Each step corresponds to the distance moved by one fluorescent peak in the cross-sectional intensity profile between consecutive frames. Our data show that the median length of a shift in 2.5s is 309 nm, but the significance of this finding remains to be explored.

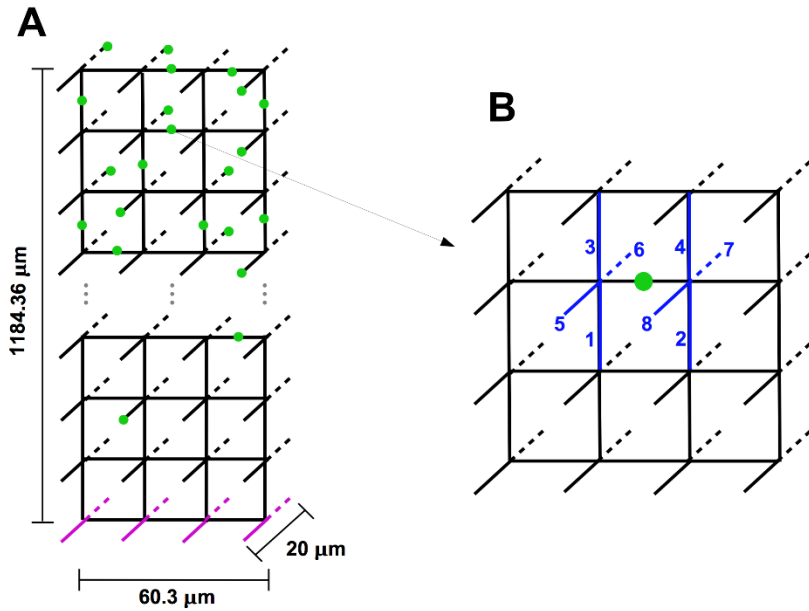


Supplemental Figure 11: Individual step sizes during fluorescent sliding. Histogram showing the number of observed occurrences of fluorescent sliding events of different lengths. The length corresponds to the absolute value of the shift of a fluorescence peak location between two consecutive images. Data in the red histogram bin corresponds to occurrences where there was no change in peak location between consecutive frames. See Supplement Section A.8 for details.

C. Mathematical Model Details

C.1 Model Overview

The stochastic model domain was a 3-dimensional square lattice (Supplemental Figure 12) with edge length 20 μm and node diameter 0.0727 nm (to mimic the length and diameter of experimental fibers). The bottom four edges of the lattice corresponded to fibrin fibers, to which plasmin could bind. A fixed number of plasmin molecules (Supplement Section C.4) were randomly uniformly distributed throughout the model domain. At each time step, each plasmin molecule had a probability of diffusing (Supplement Section C.2), and if the plasmin molecule was on an edge containing fibrin, it could bind with some probability. Bound molecules had an unbinding probability at each time step, and unbound molecules on a fibrin fiber had a binding probability (Supplement Sections C.5 and C.6). In each simulation, we recorded the location of each plasmin molecule at each time step, and whether or not each molecule was bound. This allowed us to plot time courses of the number of bound plasmin molecules, and to calculate the average time it took for plasmin to first bind to any fiber.



Supplemental Figure 12: Mathematical Model Schematic. A) Model domain. Cartoon of the model domain, which is a lattice with 60 nodes in the vertical direction and 4 nodes in the horizontal direction. Edges (black) connect adjacent nodes, and each node also contains 1 edge in the third dimension (represented by angled edges with dashed lines). The four pink edges at the bottom represent the 4 fibrin fibers; all other edges are considered "ghost edges", which do not contain fibrin. Plasmin molecules (green dots) are randomly distributed on the ghost edges. B) Schematic of where a plasmin molecule (green dot) on an interior horizontal edge can diffuse in one time step. The molecule can diffuse to one of the 8 nearest-neighbor fibers (blue). These edges are closer, diagonally, to the plasmin molecule than any other horizontal edges.

C.2 Diffusion Calculation

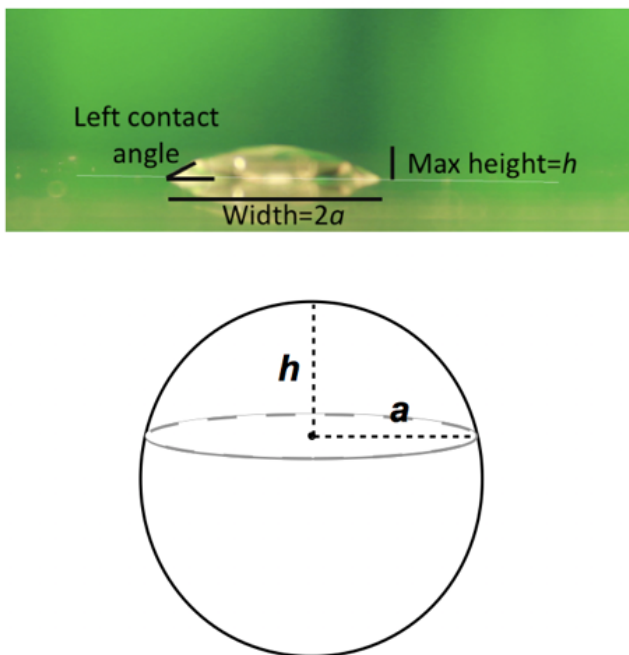
The full details of this calculation can be found in Bannish et al. [3], where "tPA" is simply replaced by "plasmin." In short, we can derive the diffusion equation, $\frac{\partial P}{\partial t} = D \nabla^2 P$, using the probability P of plasmin being on a particular lattice edge and the probability q that the plasmin molecule moves during the given time step. This probabilistic derivation allows us to associate clot features and probabilities with the deterministic diffusion coefficient:

$$D = \frac{q \times (\text{pore size})^2}{12 \Delta t}, \quad \text{or,} \quad \frac{\Delta t}{q} = \frac{(\text{pore size})^2}{12D} \quad (1)$$

For our current model, $D = 5 \times 10^{-7} \text{ cm}^2/\text{s}$ (a standard diffusion coefficient for small molecules) and pore size = 20 μm. We do not explicitly know q , the probability of a plasmin molecule moving to a neighboring edge, but it does not matter since the ratio $\Delta t/q$ is fixed. As long as we choose q such that Δt is small enough that our method converges, the actual choice of q does not matter. Model testing (not shown) indicated that $q \leq 0.02$ is sufficient, so we take $q = 0.02$ in all simulations. This means that our time step is $\frac{1}{75} \approx 0.013 \text{ s}$.

C.3 Droplet Size Calculation

The model domain size was chosen to accurately mimic the experimental conditions. Experimentally, the fibrin fibers were at the bottom of a 10 μL droplet of solution, and a second 10 μL droplet containing plasmin was added to the top of the first droplet. A Cannon EOS Rebel T6 DSLR camera was used to photograph the first droplet before and after addition of the second droplet (Supplemental Figure 13), and the droplet width and maximum height were recorded (Supplemental Table 2, n=3). The droplet shape resembled a spherical cap, located on top of the glass, which has volume $V = \frac{1}{6}\pi h(3a^2 + h^2)$, where h is the maximum height and a is the radius of the base of the cap (Supplemental Figure 13). Since we knew the volume should be 20 μL (two 10- μL droplets), we could calculate the volume of the spherical cap and confirm the experimental measurements. Results are in Supplemental Table 2. Since Droplet 1 had a calculated value much less than 20 μL , we excluded it from our calculations and took the average height of Droplets 2 and 3, approximately 1.18 mm, as the model domain height.



Supplemental Figure 13: Droplet Size. Top: Photograph of the 20 μL spherical droplet. Bottom: Cartoon showing the maximum height (h) and radius (a) of a spherical cap. Image taken with a Cannon EOS Rebel T6 DSLR camera in air with a 0.33 s exposure time and a 55mm focal length lens.

Droplet #	2a, width at base of cap (mm)	h , height (mm)	Calculated volume (μL)
1	5.65	0.88	11.39
2	6.27	1.20	19.43
3	6.66	1.15	20.83

Supplemental Table 2: Droplet Measurements.

C.4 Number of Plasmin Molecules

In the experiments, a 1.7 μM concentration of plasmin is used to initiate lysis. This corresponds to about 1024 plasmin molecules per cubic micron of clot

$$\frac{1.7 \mu\text{mol}}{\text{L}} \times \frac{1\text{L}}{10^{15} \mu\text{m}^3} \times \frac{1 \text{ mol}}{10^6 \mu\text{mol}} \times \frac{6.022 \times 10^{23} \text{ molecules}}{\text{mol}} = 1024 \frac{\text{molecules}}{\mu\text{m}^3}.$$

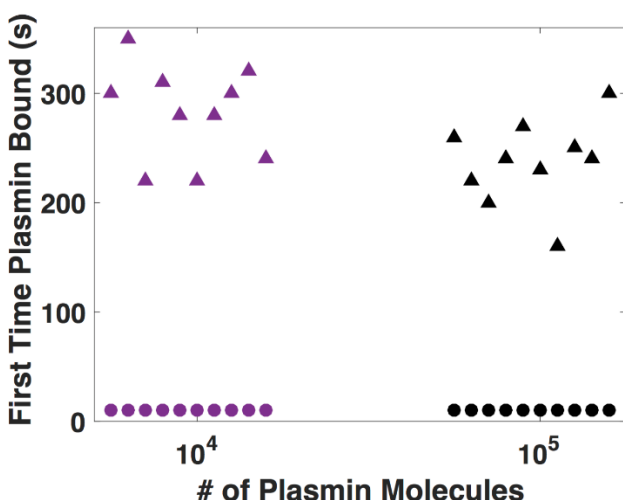
Our model clot volume is $60.3 \mu\text{m} \times 20 \mu\text{m} \times 1184.36 \mu\text{m}$, so we would need

$$1,428,338.16 \mu\text{m}^3 \times 1024 \frac{\text{molecules}}{\mu\text{m}^3} = 1,462,618,276$$

plasmin molecules to match the experimental concentration.

However, in the experiments, the plasmin is added to the pre-formed fibrin fibers in a 10 μL droplet that is gently placed on top of the existing 10 μL droplet containing the fibrin. We assume that most, but not all, of the plasmin molecules will be in the upper half of the experimental domain at time 0. We do not know exactly how many of the plasmin molecules may have started closer to the fibrin fibers (either because they were on the edge of the added droplet where it meets the fibrin-droplet, or because small-scale mixing occurs when fluid is pipetted), but we can use the model to get an estimate.

Recall that about 1.4 billion plasmin molecules should be introduced to the top half of our model domain. This is computationally intractable with the model, so we instead try two smaller amounts: 146,261 (" 10^5 " in Supplemental Figure 14) and 14,626 (" 10^4 "). We first run 10 independent simulations where we uniformly randomly initialize the plasmin just in the top half the domain, and then we run 10 more simulations in which we uniformly randomly initialize plasmin throughout the whole domain. We find that if plasmin is distributed uniformly throughout the domain, plasmin first binds to a fiber within the first 10 seconds (circles, Supplemental Figure 14), but if plasmin is only distributed in the top half of the domain, it takes on the order of 200-300 seconds for plasmin to first bind (triangles, Supplemental Figure 14). Since experimental results show fibers degrading in as fast as 15 seconds, there must be some plasmin in the bottom half of the domain, too.



Supplemental Figure 14: First Time Plasmin Bound. Time first plasmin molecule bound to a fibrin fiber in each of ten independent simulations of the mathematical model with 10^4 (purple) or 10^5 (black) plasmin molecules distributed uniformly throughout the entire domain (circles) or only in the top half (triangles).

A quick calculation lends even more credence to this assertion. Consider the plasmin molecule on the righthand diagram in Supplemental Figure 12. Since it can diffuse to one of the blue edges in the next time step, it would take two time steps for it reach the horizontal edge directly below, which is $20.0727 \mu\text{m}$ below its current position. Assuming the best-case scenario, in which the plasmin molecule is on the bottom row of the top half of the domain, it must diffuse $582.18 \mu\text{m}$ to make it to the bottom row of the clot, where the fibrin fibers are located. So, $582.18/20.0727 = 28.09$, times 2 time steps, means it would take about 56 time steps in the best-case scenario for plasmin to find a fiber. Assuming plasmin *always* chooses to move ($q=1$, see Supplement Section C.2), and it *always* moves in a direction that brings it closer to a fiber, the absolute fastest it could find the fiber is in $56 \times (2/3 \text{ s}) = 37.3 \text{ s}$. (The time step, $2/3 \text{ s}$, was calculated using Eq. (1) above.)

The above analysis leads us to conclude that there must be *some* plasmin distributed throughout the domain in the experiments, otherwise fibers would not be able to degrade in under a minute. Hence, we consider 4 different cases - which we call " 10^1 " (14 molecules, 0.000001% of the total plasmin), " 10^2 " (146 molecules, 0.00001% of the total plasmin), " 10^3 " (1462 molecules, 0.0001% of the total plasmin), and " 10^4 " (14,626 molecules, 0.001% of the total plasmin) - in which we uniformly randomly distribute the listed fraction of molecules throughout all of the ghost edges (not just the top half). The 10^3 model results best replicate experimental data, suggesting that about 0.0001% of the plasmin that is added experimentally as part of the second $10 \mu\text{L}$ droplet infiltrates the original $10 \mu\text{L}$ droplet (containing the fibrin).

C.5 Model Algorithm

- I. Create a 3-D lattice by setting the number of nodes in the horizontal and vertical directions. Connect adjacent nodes with a line segment (or "edge") to create the "horizontal" and "vertical" edges (e.g., plasmin is on a horizontal edge and edges 1, 2, 3, and 4 are vertical in Supplemental Figure 12B), and draw an edge coming out of the plane of the page at each lattice node to create the "3-dimensional" edges (e.g., edges 5, 6, 7, 8 are 3-D edges in Supplemental Figure 12B).
- II. Identify the bottom four 3-D edges as fibrin fibers (pink edges in Supplemental Figure 12A), and all remaining edges as "ghost edges".
- III. Randomly initialize the M plasmin molecules on any of the 652 ghost edges, which have been assigned a number from 1 to 652: Partition the interval $[0,1]$ into 652 equal subintervals, and select M random numbers from a uniform distribution. Find the subinterval in which each random number falls, and place one plasmin molecule on the correspondingly-numbered ghost edge. All these molecules are initially unbound, as they can only bind to fibrin fibers, not ghost edges.

IV. At each time step (time step derived in Supplement Section C.2):

1. Update the current time, t : $t = \text{previous time} + \text{time step}$.
2. For each plasmin molecule, check if the molecule is bound.
 - a. If yes, check if the molecule's unbinding time is less than the current time.
 - i. If yes, unbind the molecule and calculate a new binding time as described in step IV2biiB1IICii below.
 - ii. If no, leave bound.
 - b. If no, check if the molecule will move this time step by choosing a uniformly distributed random number, r , and comparing it to the probability of staying, $1 - q$:
 - i. If $r \leq 1 - q$ (where q is the probability of moving in a given time step as described in Supplement Section C.2), then the molecule stays on the current edge.
 - A. If the current edge is a ghost edge, the molecule remains unbound.
 - B. If the current edge is a fibrin fiber, check if the molecule's binding time is less than the current time.
 1. If yes, have the molecule bind, reset its binding time to 0, and calculate its unbinding time as $t_{\text{unbind}} = t + \frac{1}{k_{\text{off}}} - 0.5 \times (\text{time step})$, where t is the current time and we subtract half a time step so that we round to the nearest time step. k_{off} is the kinetic unbinding rate of plasmin from fibrin, taken to be 0.05s^{-1} , so $1/k_{\text{off}}$ is the average time a plasmin molecule stays bound.
 2. If no, molecule remains unbound at current edge.
 - ii. If $r > 1 - q$, then the molecule can move to one of the neighboring edges.
 - A. If molecule is on a ghost edge, it cannot bind, so its only option is to move. Jump to steps IV2biiB1IIa-IV2biiB1IIc below.
 - B. If the molecule is on a fibrin fiber, randomly decide whether the molecule binds or moves.

1. If the molecule's binding time is less than the current time but greater than 0, choose a uniformly distributed random number, r_1 .
 - I. If $r_1 \leq \frac{\text{current time} - \text{binding time}}{\text{time step}}$, the molecule binds to the fiber, we reset the binding time to 0, and we calculate the unbinding time as in step IV2biB1 above.
 - II. If $r_1 > \frac{\text{current time} - \text{binding time}}{\text{time step}}$, the molecule moves before it has a chance to bind. To determine which of the neighboring edges the molecule moves to:
 - a. Partition the interval $[0, 1]$ into X equal subintervals, where X is the number of neighboring fibers the molecule could diffuse to in one time step ($X=8$ in Supplemental Figure 12B).
 - b. Choose a uniformly distributed random number, r_2 , and determine in which of the X subintervals it falls; the correspondingly-numbered edge is the one to which the molecule moves.
 - c. Move the molecule to the new edge.
 - i. If the new edge is a ghost edge, we are done.
 - ii. If the new edge is a fibrin fiber, calculate the molecule's binding time from an exponential distribution (minus a half time step so we round to nearest time step): $\text{binding time} = t - \frac{\log(r_3)}{k_{\text{on}} \cdot bs} - 0.5$ · (time step), where r_3 is a uniformly distributed random number, k_{on} is the kinetic binding rate of plasmin to fibrin (taken to be $0.1 \mu\text{M}^{-1}\text{s}^{-1}$), and bs is the concentration of binding sites (taken to be $427 \mu\text{M}$).
2. If the molecule's binding time is 0 or greater than the current time, it cannot bind this time step, so the only option is movement. Follow steps IV2biiB1IIa-IV2biiB1IIc above.
3. Once steps IV2a and IV2b have been completed for every plasmin molecule, return to step IV1 and repeat.
4. Continue until some prescribed final time is reached.

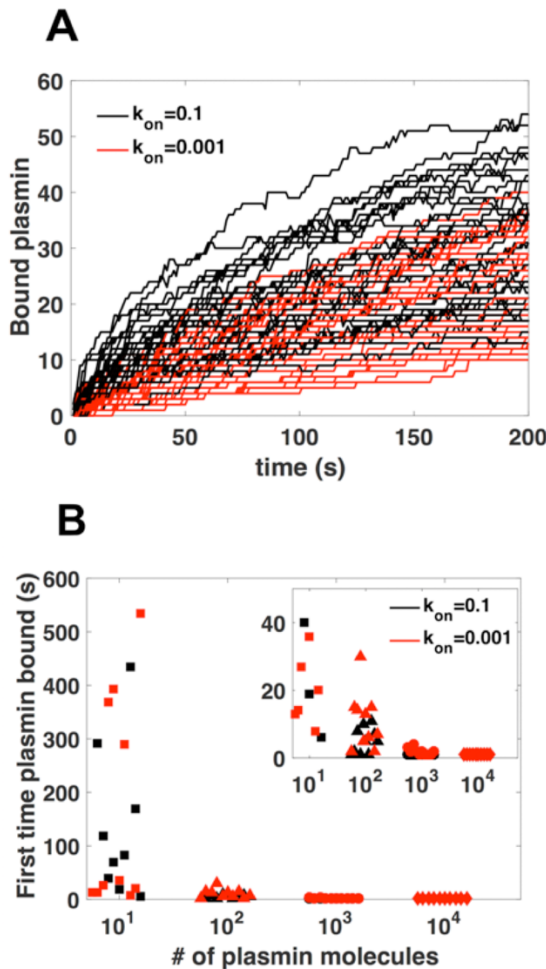
C.6 Plasmin Binding Rate Results

For simulations presented in this paper, model parameters were fixed at the values give in Supplemental Table 3. However, a convenient feature of the model is that any of

these parameter values can be easily changed and new results generated. Supplemental Figure 15 shows results from using two different k_{on} values, while keeping the dissociation constant fixed: $k_{\text{on}} = 0.1 \mu\text{M}^{-1}\text{s}^{-1}$ (the baseline value used in this paper) and $k_{\text{on}} = 0.001 \mu\text{M}^{-1}\text{s}^{-1}$. Unsurprisingly, we notice that with the smaller k_{on} value (red symbols and curves in Figure 15), plasmin is a little slower to bind, and there are fewer bound plasmin molecules after 50 s compared to the larger k_{on} case (8.45 vs. 14.25 molecules, on average).

Description	Symbol	Value
Diameter	d	$0.0727 \mu\text{m}$
Pore size	ps	$20 \mu\text{m}$
Plasmin binding rate	k_{on}	$0.1 \mu\text{M}^{-1}\text{s}^{-1}$
Plasmin unbinding rate	k_{off}	0.05 s^{-1}
Binding site conc.	bs	$427 \mu\text{M}$
Diffusion coefficient	D	$5 \times 10^{-7} \text{ cm}^2/\text{s}$
Probability of moving	q	0.02
# of plasmin molecules	M	1,462*

Supplemental Table 3: Model parameter values. *The default number of plasmin molecules was 1,462, however a range of values from 14 to 146,261 was used to make Figure 3B and Supplemental Figures 14&15.



Supplemental Figure 15: Model Results For Different Plasmin Binding Rates. A) Time course of plasmin binding to fibrin fibers. Individual curves show the data for the number of plasmin molecules bound to a distinct fiber as a function of time for simulations with $k_{on} = 0.1 \mu\text{M}^{-1}\text{s}^{-1}$ (black) and $k_{on} = 0.001 \mu\text{M}^{-1}\text{s}^{-1}$ (red). Each of the 10 independent simulations for each k_{on} value included 4 fibrin fibers and was initialized with 1426 plasmin molecules randomly distributed throughout the domain. B) The time at which plasmin first bound to any fiber, as a function of the order-of-magnitude number of plasmin molecules used in the simulation. 10 independent simulations were run for each plasmin amount (different symbols), for $k_{on} = 0.1 \mu\text{M}^{-1}\text{s}^{-1}$ (black) and $k_{on} = 0.001 \mu\text{M}^{-1}\text{s}^{-1}$ (red). Inset is zoomed in version of larger figure.

References

Reference List

- [1] C.A. Schneider, W.S. Rasband, K.W. Eliceiri, NIH Image to ImageJ: 25 years of image analysis, *Nature methods*. 9 (2012) 671-675.
- [2] J. Schindelin, I. Arganda-Carreras, E. Frise, V. Kaynig, M. Longair, T. Pietzsch, S. Preibisch, C. Rueden, S. Saalfeld, B. Schmid, J. Tinevez, D.J. White, V. Hartenstein, K. Eliceiri, P. Tomancak, A. Cardona, Fiji: an open-source platform for biological-image analysis, *Nature methods*. 9 (2012) 676-682.

- [3] B.E. Bannish, J.P. Keener, A.L. Fogelson, Modelling fibrinolysis: a 3D stochastic multiscale model, *Mathematical medicine and biology*. 31 (2014) 17-44.

Supplemental Video Captions

Supplemental Video 1. This video shows a fibrin fiber undergoing digestion by plasmin until the time immediately before the fiber is cleaved. Dimming of the fiber is the digestion by plasmin. Key characteristics are the large digestion site on the middle left section of the fiber which towards the end of the time series clearly shows fluorescence sliding away from that site. There are other notable sites of digestion to the left of the major digestion site and on the right side of the fiber.

Supplemental Video 2. This video shows a fibrin fiber undergoing digestion by plasmin until the time immediately before the fiber is cleaved. Dimming of the fiber is the digestion by plasmin. Key characteristics are the large digestion sites on the left and middle right side of the fiber and the substantial fluorescent sliding away from the major digestion site on the left.

Supplemental Video 3. This video shows a fibrin fiber undergoing digestion by plasmin until the time immediately before the fiber is cleaved. Dimming of the fiber is the digestion by plasmin. One key characteristic is the sliding seen in the final frames of the video due to the major digestion site in the middle of the fiber. Also noteworthy are the multiple digestion sites that begin to present themselves in the final frames before the fiber is lysed.

Supplemental Video 4. This video shows a fibrin fiber undergoing digestion by plasmin until the time immediately before the fiber is cleaved. Dimming of the fiber is the digestion by plasmin. Key characteristics are the major digestion sites that form on the right and left side of the fiber. Curiously there was little fluorescent sliding with this fiber, perhaps suggesting it was under lower tension.

Supplemental Video 5. This video shows a fibrin fiber undergoing digestion by plasmin until the time immediately before the fiber is cleaved. Dimming of the fiber is the digestion by plasmin. Key characteristics are the main digestion site on the right side of the fiber which causes most of the fluorescent sliding (away from that site) and the multitude of digestion sites that become visible during the last few frames of digestion.